

Davis-Greenstein alignment of oblate spheroidal grains

W. G. Roberge¹ & A. Lazarian²

to appear in *Monthly Notices of the Royal Astronomical Society*

ABSTRACT

We present extensive calculations on the efficiency of grain alignment by the Davis-Greenstein mechanism. We model the grains as oblate spheroids with arbitrary axis ratios. Our description of the grain dynamics includes (i) magnetic dissipation and the inverse process driven by thermal fluctuations in the grain magnetization; (ii) gas-grain collisions and thermal evaporation of molecules from the grain surface; (iii) the transformation of rotational energy into heat by the Barnett effect and the inverse process driven by thermal fluctuations; and (iv) rapid Larmor precession of the grain angular momentum about the interstellar magnetic field. For ordinary paramagnetic grains, we calculate the Rayleigh reduction factor, R , for >1000 combinations of the 3 dimensionless parameters which characterise the alignment. For superparamagnetic grains, we calculate R from an exact analytic solution for the relevant distribution function. Our results are compared with classical studies of DG alignment, which did not include the Barnett effect. We calibrate the accuracy of a recently-proposed perturbative approximation, which includes the Barnett effect, and show that it yields R values with a mean error of $\approx 17\%$.

Subject headings: dust — polarization — ISM: continuum — ISM: magnetic fields

1. Introduction

Nearly half a century after the discovery of interstellar polarization, the alignment of interstellar dust grains remains poorly understood. One candidate for the mysterious alignment mechanism is a process described by Davis and Greenstein (1951, henceforth DG51), in

¹Dept. of Physics, Applied Physics & Astronomy, Rensselaer Polytechnic Institute, Troy, NY 12180, USA, roberw@rpi.edu

²Dept. of Astrophysical Sciences, Princeton University; Current address: Canadian Institute for Theoretical Astrophysics, University of Toronto, Toronto, Ontario, Canada M5S 3H8; lazarian@cita.utoronto.ca

which paramagnetic dissipation aligns the grain angular momentum, \mathbf{J} , with the interstellar magnetic field, \mathbf{B} . The alignment of the grain *axes* with \mathbf{B} requires a correlation between \mathbf{J} and the axial directions. In the original formulation of DG51, the required correlation is produced by the torques due to paramagnetic dissipation and gas damping. The Davis-Greenstein (DG) mechanism was subsequently modified to describe ferromagnetic grains (Spitzer & Tukey 1951) and to include the important disorienting effects of thermal fluctuations in the magnetization (Jones & Spitzer 1967, henceforth JS67). The “classical age” of grain alignment research culminated with extensive quantitative investigations based on the Fokker-Planck equation (JS67) and Monte Carlo methods (Purcell 1969; Purcell & Spitzer 1971, henceforth PS71). These studies concluded that the DG mechanism can explain the polarization observed toward diffuse clouds if the grains are superparamagnetic, but requires magnetic fields $> 10^{-5}$ G if the grains are composed of ordinary paramagnetic substances.

The classical era was followed by a twenty-year period with little research on the DG effect, during which interest focussed on an alternative mechanism proposed by Purcell (1979, henceforth P79). In Purcell’s mechanism, magnetic dissipation aligns the angular momenta with \mathbf{B} , as in DG51, but rotation at superthermal energies stabilizes the grains against disorientation by the gas particles. P79 also showed that the “internal alignment” of the grain axes with \mathbf{J} is determined by the conversion of rotational energy into heat via frictional processes internal to the grain (e.g., the Barnett effect). Internal dissipation drives an isolated grain toward the state of minimum energy consistent with angular momentum conservation. For rotational energies much larger than the equipartition energy, the result is almost perfect alignment between \mathbf{J} and the principal axis of largest rotational inertia.

Research on the DG mechanism has been reinvigorated by studies of polarization toward molecular clouds, where the physical conditions appear unfavorable for Purcell’s mechanism (and other mechanisms, see Hildebrand 1988, 1996 and references therein). Roberge, DeGraff and Flaherty (1993, henceforth RDGF93) modified the DG effect to include internal dissipation in the regime where the internal alignment is perfect. Lazarian (1995, henceforth L95) presented an accurate analytic solution for the alignment efficiency in this regime. Detailed studies of internal dissipation (Lazarian 1994; Lazarian & Roberge 1997, henceforth L94 and LR97, respectively) showed that internal alignment becomes imperfect at thermal rotation energies and produced an accurate quantitative theory of the dissipation mechanism. The modification of the DG effect to include imperfect internal alignment was carried out by Lazarian (1997, henceforth L97), who gave an approximate analytic solution of the Fokker-Planck equation.

The approach of L97 replaces certain random variables in the Fokker-Planck equation with their mean values. Though physically well motivated, this is an ad hoc approximation

whose accuracy can only be determined by comparison with calculations of known accuracy. In this paper we present such calculations. Our plan is as follows: The dynamical processes and modelling assumptions included in our calculations are summarised in §2. In §3 we describe an adiabatic approximation (Roberge 1997, henceforth R97) that yields accurate solutions of the Fokker-Planck equation along with a rigorous procedure for estimating the errors. In §4 we evaluate these solutions numerically for ordinary paramagnetic grains (§4.1) and analytically for superparamagnetic grains (§4.2). We compare our results with the classical studies of DG alignment in §5.1 and with the results of L97 in §5.2. The status of the DG mechanism, including outstanding problems, is discussed in §6 and our results are summarised in §7.

2. Modelling assumptions

2.1. Grain model

We model the grains as oblate spheroids with semiaxes a parallel to the symmetry axis and b perpendicular to the symmetry axis. Let $\{\hat{\mathbf{x}}^b, \hat{\mathbf{y}}^b, \hat{\mathbf{z}}^b\}$ be the Cartesian basis of a “body frame” attached to the grain, where $\hat{\mathbf{z}}^b$ is parallel to the symmetry axis, \mathbf{a} (Fig. 1). The components of the inertia tensor for rotation parallel and perpendicular to $\hat{\mathbf{z}}^b$ will be denoted I_{\parallel} and I_{\perp} , respectively. Our model grains are composed of an unspecified solid with uniform density ρ_s , temperature T_s , and frequency-dependent magnetic susceptibility $\chi(\omega) = \chi'(\omega) + i\chi''(\omega)$. They are located in a static gas of particles with mass m , number density n , and kinetic temperature T_g , plus a uniform magnetic field, \mathbf{B} .

2.2. Dynamical processes

We are interested ultimately in the distribution of the grain orientations in an inertial frame fixed to the gas. Let $\{\hat{\mathbf{x}}, \hat{\mathbf{y}}, \hat{\mathbf{z}}\}$ be the basis of the inertial frame, with $\hat{\mathbf{z}}$ parallel to \mathbf{B} and the other basis vectors oriented arbitrarily in the plane perpendicular to \mathbf{B} (Fig. 2). The orientation of \mathbf{a} in the inertial frame changes due to (i) the motion of the grain’s axes with respect to \mathbf{J} caused by rotation and the Barnett effect, plus (ii) the motion of \mathbf{J} in the inertial frame caused by Larmor precession and the DG effect. It is therefore natural to specify the orientation in terms of the four angles defined in Figures 1 and 2, so that (θ, ψ) gives the orientation of \mathbf{a} with respect to \mathbf{J} and (β, ϕ) gives the orientation of \mathbf{J} with respect to \mathbf{B} .

The dynamical timescales for these variables are listed in Table 1. The rotational motion

of a spheroid causes \mathbf{a} to precess about \mathbf{J} with period $\sim t_{\text{rot}}$ (for reasonable grain shapes) and the interaction of the grain magnetic moment with the interstellar magnetic field causes \mathbf{J} to precess about \mathbf{B} with period t_{Lar} . The smallness of the rotation and Larmor periods compared to all other timescales of interest insures that ψ and ϕ are uniformly distributed. Thus, only the joint distribution of θ and β needs to be calculated in practice.

We assume that internal dissipation is dominated by the Barnett effect¹, which therefore determines the motion of θ .² The systematic and random motions of θ produced by Barnett dissipation and thermal fluctuations in the Barnett magnetization (collectively termed “Barnett relaxation”) have dynamical timescale

$$t_{\text{Bar}} = \frac{\mu^2 I_{\parallel}^3}{VKh^2(h-1)J^2} \quad (2-1)$$

(RDGF93), where V is the grain volume, $h \equiv I_{\parallel}/I_{\perp}$, $K \equiv \chi''/\omega$ and μ is the magnetogyric ratio of the orientable spins or orbits responsible for the Barnett magnetization. The Barnett time depends on the angular momentum; the value given in Table 1 was computed for a grain with J equal to

$$J_{\text{th}} \equiv \sqrt{I_{\parallel} k T_{\text{g}}}, \quad (2-2)$$

a typical value for thermal rotation.

We assume that the motion of β is caused by (i) the systematic and random torques produced by gas-grain collisions and thermal evaporation of molecules from the grain surface (“gas damping”); and (ii) the systematic and random torques produced by paramagnetic or superparamagnetic relaxation (“magnetic damping”). The gas damping time is the timescale for \mathbf{J} to be reduced by rotational friction with the gas. For a spheroid rotating about its symmetry axis,

$$t_{\text{gas}} \equiv \frac{3I_{\parallel}}{4\sqrt{\pi}nmb^4v_{\text{th}}\Gamma_{\parallel}} \quad (2-3)$$

(RDGF93), where $v_{\text{th}} \equiv \sqrt{2kT_{\text{g}}/m}$ is the gas thermal speed and Γ_{\parallel} is a dimensionless coefficient that depends weakly on the grain shape [see eq. (A7)]. The magnetic damping

¹A recent study by Lazarian & Efroimsky (1999) shows that, for grains with large axis ratios and grains produced by agglomeration, internal dissipation is dominated by inelasticity. However, this has no effect on the conclusions of the present study, which only requires the timescale for internal dissipation to be much smaller than the timescale for external interactions.

²In principle, we should also include gas damping: the impulsive change in \mathbf{J} due to a gas-grain collision or evaporation from the grain surface changes θ . In omitting these effects we introduce errors in the θ distribution that, for typical molecular clouds, are of order $t_{\text{Bar}}/t_{\text{gas}} \sim 10^{-3}$.

time for a spheroid rotating about its symmetry axis is

$$t_{\text{mag}} \equiv \frac{I_{\parallel}}{KVB^2}. \quad (2-4)$$

The choice of a particular rotation axis for the purpose of defining characteristic timescales obviously involves no loss of generality, but must be taken into account when comparing results from different papers. In particular, PS71 defined t_{gas} and t_{mag} with respect to rotation about the *transverse* axis. To compare our results with those of PS71, it is only necessary to note that $\delta_m = (\Gamma_{\perp}/\Gamma_{\parallel}) \delta$, where Γ_{\perp} is a dimensionless function of the grain shape [see eq. (A8)], δ_m is our magnetic damping parameter [see eq. (3-17)] and δ is the magnetic damping parameter of PS71.

2.3. Characterisation of the alignment

Our objective is to calculate the quantity which characterises the mean axial alignment for an ensemble of identical grains. Because different definitions of this quantity have appeared in the literature, due to differing assumptions about the grain dynamics, a brief review of this subject is appropriate.

Consider an electromagnetic wave propagating along the \hat{z}^o axis of the Cartesian “observer frame” defined in Figure 3. The transfer equations for the Stokes parameters depend on the cross sections³ C_x^o and C_y^o for linearly polarized waves with the electric vector, \mathbf{E} , along the \hat{x}^o and \hat{y}^o directions (e.g., see Martin 1974, Lee & Draine 1985). To calculate these “observer frame” cross sections, one transforms the components of \mathbf{E} to a frame aligned with the principal axes of the grain and takes the appropriately-weighted sum of the cross sections, C_{\parallel} and C_{\perp} , for \mathbf{E} polarized along the grain axes. When the transformation is carried out and the resulting expressions are averaged over ψ and ϕ , one finds that the mean cross sections for an ensemble of oblate spheroids are

$$C_x^o = C_{\text{avg}} + \frac{1}{3} R (C_{\perp} - C_{\parallel}) (1 - 3 \cos^2 \zeta) \quad (2-5)$$

and

$$C_y^o = C_{\text{avg}} + \frac{1}{3} R (C_{\perp} - C_{\parallel}), \quad (2-6)$$

where $C_{\text{avg}} \equiv (2C_{\perp} + C_{\parallel})/3$ is the effective cross section for randomly-oriented grains. Grain alignment is characterised by the Rayleigh reduction factor,

$$R \equiv \langle G(\cos^2 \theta) G(\cos^2 \beta) \rangle, \quad (2-7)$$

³We use the term “cross section” generically to refer to the extinction and phase advance cross sections.

where θ is the angle between the axis of largest rotational inertia (i.e., $\hat{\mathbf{z}}^b$ for a homogeneous oblate spheroid), β is the angle between \mathbf{J} and \mathbf{B} ,

$$G(x) \equiv \frac{3}{2} \left(x - \frac{1}{3} \right) \quad (2-8)$$

and $\langle \rangle$ denotes the ensemble average. Thus, our objective is to calculate R .

Two related “alignment measures” which frequently appear in the literature are

$$Q_X \equiv \langle G(\cos^2 \theta) \rangle = \frac{3}{2} \left(\langle \cos^2 \theta \rangle - \frac{1}{3} \right), \quad (2-9)$$

which measures the mean alignment of \mathbf{a} with \mathbf{J} , and

$$Q_J \equiv \langle G(\cos^2 \beta) \rangle = \frac{3}{2} \left(\langle \cos^2 \beta \rangle - \frac{1}{3} \right), \quad (2-10)$$

which describes the alignment of \mathbf{J} with \mathbf{B} . The Rayleigh reduction factor cannot be determined uniquely from Q_J and Q_X without making additional approximations because in general θ and β are correlated. For example, if one assumes that Barnett dissipation aligns \mathbf{a} *perfectly* with \mathbf{J} (e.g., see Lee & Draine 1985; RDGF93; L95), then $G(\theta) = 1$ and $R = Q_J$. This assumption is appropriate when the grains rotate with energies $\gg kT_s$ (P79) but a poor approximation for thermal rotation, the case of interest here (L94; LR97). We make no *a priori* assumptions about a possible relationship between R , Q_X , and Q_J .

3. Mathematical formulation

3.1. The Fokker-Planck equation

Although we are interested only in the distribution of θ and β , it is easier for practical reasons to calculate the joint distribution of θ and all 3 angular momentum coordinates. Let (J_x, J_y, J_z) be the Cartesian coordinates of \mathbf{J} in the inertial frame. Define the distribution function, $f(\theta, J_x, J_y, J_z)$, so that $f(\theta, J_x, J_y, J_z) d\theta dJ_x dJ_y dJ_z$ is the joint probability of finding \mathbf{a} oriented in the infinitesimal interval $d\theta$ centered at θ and the angular momentum in $dJ_x dJ_y dJ_z$ centered at (J_x, J_y, J_z) . Then f satisfies the Fokker-Planck equation,

$$\frac{\partial f}{\partial t} = -\frac{\partial}{\partial \theta} \left[A_\theta f - \frac{\partial}{\partial \theta} (B_{\theta\theta} f) \right] - \frac{\partial}{\partial J_k} \left[A_k f - \frac{\partial}{\partial J_k} (B_{kk} f) \right], \quad (3-1)$$

where repeated indices are summed over x, y, z and we have anticipated the result [see eqs. (3-19)–(3-21)] that B is a diagonal tensor. The diffusion coefficients A_θ and $B_{\theta\theta}$, which

describe the variations in θ due to Barnett relaxation, were derived in LR97. However they are not needed in the approximation described below (see §3.2). The coefficients A_k and B_{kk} describe the analogous changes in the angular momentum components due to the combined effects of gas- and magnetic damping. They are given for reference in Appendix A. The angular momentum diffusion coefficients are functions of θ , $\{J_k\}$ and physical parameters such as the grain temperature and magnetic field strength. We assume that all physical parameters are constant over times much longer than the timescales in Table 1, so that only the steady solutions of eq. (3-1) are of interest.

3.2. Adiabatic elimination of θ

According to Table 1, the dynamical timescale for θ is typically ~ 3 orders of magnitude shorter than the timescales for the angular momentum components.⁴ It is possible to exploit this disparity to greatly simplify the calculation of f . In particular, R97 showed that

$$f(\theta, J_x, J_y, J_z) = f_{\text{int}}(\theta | J) f_{\text{ext}}(J_x, J_y, J_z) + \mathcal{O}(\epsilon), \quad (3-2)$$

where $f_{\text{int}}(\theta | J)$ can be calculated from equilibrium thermodynamics,⁵ f_{ext} satisfies a simplified Fokker-Planck equation described below and $\epsilon \sim 10^{-3}$ is the ratio of t_{Bar} to the shortest timescale for the motion of \mathbf{J} .

LR97 showed that the conditional θ distribution is

$$f_{\text{int}}(\theta | J) = C_\theta \sin \theta \exp(-\xi^2 \sin^2 \theta), \quad (3-3)$$

where C_θ is a normalization constant and

$$\xi^2 \equiv \frac{(h-1) J^2}{2I_{\parallel} k T_s}. \quad (3-4)$$

Expression (3-3) is the thermal equilibrium θ distribution for an isolated grain with fixed angular momentum. It depends parametrically on J as the notation $f_{\text{int}}(\theta | J)$ suggests. This result has an obvious physical interpretation: as the angular momentum slowly changes, the rapid evolution of θ allows f_{int} to relax adiabatically to the equilibrium distribution that would obtain if J were frozen at its instantaneous value. Consequently, we refer to expression (3-2) as the adiabatic approximation.

⁴There is no need to modify this statement if the grains are superparamagnetic, since superparamagnetism would reduce t_{mag} and t_{Bar} by the same factor.

⁵It follows that f_{int} is independent, to $\mathcal{O}(\epsilon)$, of the particulars of the relaxation mechanism.

The statistics of f_{int} are functions of J^2 . Examples that appear frequently in the following discussion are the conditional mean values of $\sin^2 \theta$,

$$\sigma \equiv \int_0^\pi \sin^2 \theta f_{\text{int}}(\theta | J) d\theta, \quad (3-5)$$

$\cos^2 \theta$,

$$\kappa \equiv 1 - \sigma, \quad (3-6)$$

and the related alignment measure

$$q_X \equiv \frac{3}{2} \left(\kappa - \frac{1}{3} \right). \quad (3-7)$$

They are plotted in Figure 4. The alignment of \mathbf{a} with \mathbf{J} is different for each grain in the ensemble, with q_X increasing from zero for grains with $J = 0$ to unity for grains with $J^2 \gg (h - 1)I_{\parallel}kT_s$. The mean alignment for the ensemble is described by Q_X , the average of q_X over the angular momentum distribution.

In the adiabatic approximation, the angular momentum distribution satisfies the Fokker-Planck equation

$$-\frac{\partial}{\partial J_k} \left[\bar{A}_k f_{\text{ext}} \right] + \frac{1}{2} \frac{\partial^2}{\partial J_k^2} \left[\bar{B}_{kk} f_{\text{ext}} \right] = 0, \quad (3-8)$$

where the coefficients \bar{A}_k and \bar{B}_{kk} are obtained by averaging the θ -dependent coefficients in expression (3-1) in the obvious way. Thus,

$$\bar{A}_k \equiv \int_0^\pi d\theta A_k f_{\text{int}}(\theta | J) \quad (3-9)$$

and

$$\bar{B}_{kk} \equiv \int_0^\pi d\theta B_{kk} f_{\text{int}}(\theta | J). \quad (3-10)$$

With θ thus eliminated, the grain alignment problem reduces to solving equation (3-8) for the angular momentum distribution. Once this is accomplished, the Rayleigh reduction factor can be found by evaluating

$$R = \int d^3J f_{\text{ext}}(J_x, J_y, J_z) q_X(J^2) G(\cos^2 \beta), \quad (3-11)$$

where \int denotes the definite integral over all of angular momentum space.

3.3. Dimensionless parameters

We minimize the number of independent parameters in the problem by writing \bar{A} and \bar{B} in terms of dimensionless units, with angular momentum measured in units of J_{th} and time

measured in units of t_{gas} . Henceforth it is implied that all quantities are in dimensionless units unless it is explicitly stated otherwise.

After evaluating expression (3-9) and writing the result in dimensionless form, one finds that the mean torque has components

$$\bar{A}_x = -k_{xy} J_x, \quad (3-12)$$

$$\bar{A}_y = -k_{xy} J_y \quad (3-13)$$

and

$$\bar{A}_z = -k_z J_z. \quad (3-14)$$

The damping rates,

$$k_{xy} \equiv 1 + \delta_m + [\lambda + (h - 1)\delta_m] \sigma \quad (3-15)$$

and

$$k_z \equiv 1 + \lambda \sigma, \quad (3-16)$$

are functions of J^2 (through σ). They depend also on the magnetic damping parameter,

$$\delta_m \equiv \frac{t_{\text{gas}}}{t_{\text{mag}}}, \quad (3-17)$$

and the dimensionless shape parameters $h - 1$ and

$$\lambda \equiv h\Gamma_{\perp}/\Gamma_{\parallel} - 1 \quad (3-18)$$

(see Fig. 5).

The evaluation of the diffusion tensor yields

$$\bar{B}_{xx} = (1 + T_s/T_g) (1 - \gamma \eta_{xy}) + 2 (T_s/T_g) \delta_m, \quad (3-19)$$

$$\bar{B}_{yy} = \bar{B}_{xx} \quad (3-20)$$

and

$$\bar{B}_{zz} = (1 + T_s/T_g) (1 - \gamma \eta_z) + 2 (T_s/T_g) \delta_m, \quad (3-21)$$

where

$$\gamma \equiv 1 - \Gamma_{\perp}/\Gamma_{\parallel} \quad (3-22)$$

is a dimensionless function of the grain shape (Fig. 5). The diffusion tensor depends on J^2 and $\cos^2 \beta$ via the coefficients

$$\eta_{xy} (J^2, \cos^2 \beta) \equiv \frac{1}{2} \left[1 + \cos^2 \beta + \frac{1}{2} \sigma (1 - 3 \cos^2 \beta) \right] \quad (3-23)$$

and

$$\eta_z (J^2, \cos^2 \beta) \equiv 1 - \cos^2 \beta - \frac{1}{2} \sigma (1 - 3 \cos^2 \beta). \quad (3-24)$$

We conclude that the diffusion coefficients, and therefore R , depend on T_s/T_g , δ_m and 3 dimensionless functions of the grain shape. We will parameterize our solutions by T_s/T_g , δ_m and a/b .

4. Results

4.1. Ordinary paramagnetic grains

Equation (3-8) must be solved numerically in general. We do this using an algorithm described in RDGF93, to which we refer the reader for a thorough description of the method. In brief, we exploit the mathematical equivalence of eq. (3-8) and the coupled Langevin equations

$$dJ_k = \bar{A}_k dt + \sqrt{\bar{B}_{kk}} dW_k \quad (\text{no summation on } k), \quad (4-1)$$

where $\{dW_k\}$ are independent Gaussian random variables with variance dt . We integrate these equations numerically as an initial value problem to generate simulations of the time-dependent angular momentum components and compute statistics of the angular momentum distribution, such as R , by equating time- and ensemble averages. Theorems insure that our statistics converge to their exact values in the limits $\Delta t \rightarrow 0$ and $T \rightarrow \infty$, where Δt is the time step and T is the total averaging time. The benchmark tests and “production” calculations reported in this paper use $\Delta t = 10^{-3}$ and $T = 10^5$ dimensionless units unless it is stated otherwise.

Because we are interested only in statistics of the steady-state distribution, the initial conditions on eq. (4-1) are arbitrary. Our results were obtained by initially setting the magnitude of \mathbf{J} to unity and choosing its direction randomly from an isotropic distribution. To allow our simulated grains to “forget” these initial conditions, we integrated the Langevin equations for 1000 dimensionless time units before commencing our calculation of the time averages.

Useful checks on our numerics are provided by special cases where analytic solutions for certain statistics exist. For example, Q_J can be calculated exactly for the special case $a/b = 1$ (i.e., for spherical grains; see JS67, PS71). Let \tilde{Q}_J (a random variable) denote the estimate of Q_J predicted by one numerical integration with $T = 10^5$ and $\delta Q_J \equiv \tilde{Q}_J - Q_J$ be the corresponding error. In Figure 6 we plot the error distribution obtained from 100 numerical integrations with $a/b = 1$ and the other parameters set arbitrarily to $\delta_m = 1$ and

$T_s/T_g = 0.5$. The mean and rms errors are $\overline{\delta Q_J} = -1.5 \times 10^{-4}$ and $(\overline{\delta Q_J^2})^{1/2} = 1.2 \times 10^{-3}$, respectively. We infer that the uncertainty in Q_J is dominated by statistical fluctuations in the simulations rather than systematic errors in the numerics.

In the limit $T_s/T_g \rightarrow 0$, the alignment of \mathbf{a} with \mathbf{J} becomes perfect and $R \rightarrow Q_J$. L95 developed a perturbative approximation which calculates Q_J in this regime. Figure 7 compares results obtained with our numerical method for the case $T_s/T_g = 0$, $a/b = 2/3$ (symbols) and results obtained with the perturbative approximation in fifth order (solid curve). The mean and rms discrepancies between the 49 numerical points and the corresponding predictions of perturbation theory are $\overline{\delta Q_J} = 1.2 \times 10^{-2}$ and $(\overline{\delta Q_J^2})^{1/2} = 1.3 \times 10^{-2}$. These discrepancies should be interpreted as upper limits on the errors in the numerical results, since they are due to the combined effects of errors in the numerics and the finite accuracy of the perturbation method.

Another check on the numerics is provided by the case $T_s/T_g = 1$, where the angular momentum distribution is Maxwellian and Q_X can be calculated exactly (see JS67). Figure 8 shows the errors in Q_X for 100 trials with $T_s/T_g = 1$ and the other parameters arbitrarily chosen to be $a/b = 0.5$ and $\delta_m = 1$. The mean and rms errors are $\overline{\delta Q_X} = -5 \times 10^{-4}$ and $(\overline{\delta Q_X^2})^{1/2} = 5 \times 10^{-4}$, respectively.

There do not appear to be any benchmarks that would permit us to calibrate the errors in R —the quantity of ultimate interest—for more general cases. However rough estimates can be obtained by assuming (albeit somewhat unrealistically, see the discussion below) that θ and β are uncorrelated. With this assumption, one can easily show that the mean square error in R satisfies

$$\overline{\delta R^2} = Q_J^2 \times \overline{\delta Q_X^2} + Q_X^2 \times \overline{\delta Q_J^2} + \text{terms}, \quad (4-2)$$

where the omitted terms involve higher-order products of the small quantities δQ_J and δQ_X . If we use the fact that Q_J and Q_X cannot exceed unity and assume, reasonably, that the values of $\overline{\delta Q_J^2}$ and $\overline{\delta Q_X^2}$ from the benchmarks above are typical, then

$$(\overline{\delta R^2})^{1/2} \lesssim 1 \times 10^{-3}. \quad (4-3)$$

Thus, we estimate a typical error in R to be a few units in the third decimal place.

We have computed the alignment of ordinary paramagnetic grains for 1259 parameter combinations on the uniform grids $a/b = 0.1 (0.2) 0.9$, $T_s/T_g = 0 (0.1) 0.9$, and $\log \delta_m = -1 (0.1) 1.5$. Our results are given in Tables 2–6.⁶ We have deleted the table entries whenever

⁶ These data are also available in electronic form; inquiries should be directed to WR.

$R < 5 \times 10^{-3}$, consistent with our error estimate. Davis-Greenstein alignment with R values in the omitted range may be relevant to polarization in the 2175 Å extinction feature, which has been attributed to magnetically-aligned graphite grains with $R = 1-2 \times 10^{-3}$ (Wolff et al. 1997). This hypothesis is examined in a forthcoming paper (Roberge & Karcz, in preparation), where DG alignment of graphite grains is studied using perturbation theory.

The dependence of various alignment measures on the parameters is shown in Figures 9–11. The effects of Barnett relaxation on the grain dynamics are illustrated by the graphs of Q_X . Barnett dissipation generally enhances the alignment of \mathbf{a} with \mathbf{J} , in the sense that Q_X is typically several times larger than the Q_X value for a Maxwellian distribution. Thermal fluctuations in the Barnett magnetization account for the systematic dependence of Q_X on the parameters. These fluctuations cause random changes $\sim kT_s$ in the rotational energy,

$$E_{\text{rot}} = \frac{J^2}{2I_{\parallel}} [1 + (h - 1) \sin^2 \theta]. \quad (4-4)$$

The resulting variations in θ inhibit the alignment of \mathbf{a} with \mathbf{J} unless

$$\frac{2I_{\parallel}kT_s}{(h - 1)J^2} \ll 1, \quad (4-5)$$

that is, unless kT_s is much smaller than the difference between the minimum ($\theta = 0$) and maximum ($\theta = \pi/2$) rotational energies. It follows from equation (4-5) that Q_X should decrease as the grains become more spherical (so that $h \rightarrow 1$), as the magnetic damping parameter increases (so that the mean value of J^2 decreases) and as the dust temperature increases. These trends are present in Figures 9, 10 and 11, respectively. The graphs of Q_X also provide additional checks on our calculations. Thus, Q_X vanishes in the limit $a/b \rightarrow 1$ (spherical grains disoriented completely by an infinitesimal fluctuation) and Q_X approaches the Maxwellian solution as $T_s/T_g \rightarrow 1$.

The graphs of Q_J provide similar insight. The alignment of \mathbf{J} with \mathbf{B} is nearly independent of the grain shape, Q_J being very close to the “spherical solution” for all values of the axis ratio (Fig. 9), magnetic damping parameter (Fig. 10) and dust-to-gas temperature ratio (Fig. 11). This is clearly a consequence of the weak dependence of the angular momentum diffusion coefficients on the grain shape and orientation.⁷ The monotonic increase of Q_J with δ_m (Fig. 10) reflects the increasing efficiency of magnetic damping as the ratio $t_{\text{gas}}/t_{\text{mag}}$ increases. Of course, the alignment should saturate, with Q_J approaching some asymptotic limit as $\delta_m \rightarrow \infty$. However, the largest δ_m values in Fig. 10 are too small to see this limiting

⁷ This weak dependence made the perturbative approach of L95 and L97 possible.

behavior, which is manifested only for the very large δ_m values characteristic of superparamagnetic grains (see §4.2). The rapid decline of Q_J with increasing dust temperature (Fig. 11) illustrates the effects of thermal fluctuations in the magnetization, whose interaction with \mathbf{B} produces random torques that tend to disorient \mathbf{J} (JS67). As $T_s/T_g \rightarrow 1$, a balance is reached between the dissipation of rotational energy into heat by magnetic dissipation and the transfer of energy to rotation by the fluctuations. In this limit, the distribution of the transverse angular momentum components becomes Maxwellian and the alignment of \mathbf{J} vanishes. Our solutions also satisfy this benchmark.

Our numerical code also calculates the correlations between θ and β . Define the dimensionless “correlation function” by

$$\rho \equiv \frac{\langle \cos^2 \theta \cos^2 \beta \rangle}{\langle \cos^2 \theta \rangle \langle \cos^2 \beta \rangle} - 1. \quad (4-6)$$

In Figure 12 we plot ρ vs. δ_m for the case $a/b = 2/3$ and $T_s/T_g = 0.2$. The correlations appear to be a minor effect, in the sense that $\langle \cos^2 \theta \cos^2 \beta \rangle$ never differs by more than a few percent from the product $\langle \cos^2 \theta \rangle \times \langle \cos^2 \beta \rangle$. However the apparent smallness of ρ is misleading. Let

$$R \equiv Q_X Q_J (1 + \tau), \quad (4-7)$$

so that $\tau = 0$ corresponds to the situation where the correlations vanish. It is easy to show from expressions (2-7)–(2-10) that ρ and τ are related by

$$\tau = \frac{1 + 2Q_X + 2Q_J + 4Q_X Q_J}{4Q_X Q_J} \rho, \quad (4-8)$$

so that $\tau \gg \rho$ if $Q_X Q_J \ll 1$. For example, consider the case $\delta_m = 1$, $T_s/T_g = 0.2$ and $a/b = 2/3$. The alignment measures are $Q_X = 0.1573$, $Q_J = 8.761 \times 10^{-2}$, $R = 2.376 \times 10^{-2}$ and the correlation function is $\rho = 0.025$. Thus, R is a factor ≈ 1.7 larger than the product $Q_X Q_J$ even though $\rho \ll 1$. By this measure the correlations are large. In fact, this example is typical. For the 239 data points in Figures 9–11, the ratio $R/Q_X Q_J$ varies from 1.3 to 5.0 with a mean value of 1.7. In contrast, ρ , never exceeds 0.1. We conclude that the Rayleigh reduction factor is very sensitive to small correlations between θ and β .

Because R is sensitive to the correlations, it is important to ask whether they are real or merely an artifact of the numerics. The benchmark calculations in Figs. 6–8 do not address this question because they describe special cases where the correlations vanish. Nevertheless, it is easy to see that the behavior of ρ in Fig. 12 is qualitatively correct: In the adiabatic approximation, the correlation function is merely a statistic of the angular momentum distribution, f_{ext} . We cannot check the δ_m dependence of f_{ext} directly because our numerical integration scheme yields only statistics of the various distributions. However,

there can be no qualitative differences between the δ_m dependence of f_{ext} for grains with $a/b = 2/3$ and f_{ext} for spherical grains (which can be calculated exactly, see PS71). The dashed curve in Figure 12 is an approximation to the correlation function obtained by replacing f_{ext} with the exact solution for spheres with $\delta_m = 1$ and $T_s/T_g = 0.2$.⁸ The qualitative similarity of the two curves in Fig. 12 shows that the correlations are not a numerical artifact. An additional check on the correlations is discussed in §4.2, where we show that numerically-computed R values converge to an analytic solution for R that becomes exact in the limit $\delta_m \rightarrow \infty$. Given the sensitivity of R to the correlations, the convergence can only occur if the numerical treatment of the correlations is highly accurate.

4.2. Superparamagnetic grains

The magnetic susceptibility of interstellar grains can be enhanced to “superparamagnetic” values if the grains contain small clusters of ferromagnetic or ferrimagnetic atoms (JS67; Draine 1996; Draine & Lazarian 1998, henceforth DL98). The existence of superparamagnetic grains is consistent with the wavelength dependence of continuum polarization (Mathis 1986) and is supported by the presence of small FeNi and FeNiS inclusions in the GEMS component of interplanetary dust⁹ (Bradley 1994; Martin 1995; Goodman & Whittet 1995). The alignment of superparamagnetic grains is therefore of considerable interest.

Superparamagnetism corresponds to the case $1 \ll \delta_m \lesssim 10^5$, a regime where numerical calculations of the alignment are impractical. The numerical difficulties are caused by the disparity between the timescales for gas damping ($=1$ in dimensionless units) and magnetic damping ($=\delta_m^{-1}$). (That is, the Langevin equation becomes “stiff.”) To produce accurate statistics, numerical integrations must be carried out with a timestep much smaller than the smallest dynamical timescale and an averaging time much larger than the largest timescale. It follows that the number of arithmetic operations per R value increases in proportion to δ_m and a numerical investigation of superparamagnetic alignment would require orders of magnitude more computation than the present study.

However, the disparity between t_{gas} and t_{mag} can be turned to advantage using the adiabatic elimination technique. In Appendix B we carry out the analysis to show that

$$f_{\text{ext}} = f_{xy}(J_x, J_y | J_z) f_z(J_z) + \mathcal{O}(\delta_m^{-1}). \quad (4-9)$$

⁸That is, we computed $\langle \cos^2 \theta \rangle$, etc using expressions (3-5)–(3-7) for nonspherical grains with $a/b = 2/3$ and $T_s/T_g = 0.2$ and averaged these expression over the angular momentum distribution for spheres.

⁹DL98 claim, however, that not more than 5% of interstellar iron can be in the form of metallic inclusions.

The angular momentum distribution functions, f_{xy} and f_z , have closed-form solutions. For the transverse components, we find

$$f_{xy}(J_x, J_y | J_z) = C_{xy} \exp(-\Phi), \quad (4-10)$$

where C_{xy} (a function of J_z) is determined by the normalization condition

$$\int_{-\infty}^{+\infty} \int_{-\infty}^{+\infty} f_{xy}(J_x, J_y | J_z) dJ_x dJ_y = 1. \quad (4-11)$$

The argument of the exponential is

$$\Phi(J_x, J_y | J_z) \equiv \left(\frac{T_g}{T_s}\right) \int_0^{J_\perp} [1 + (h-1)\sigma(J')] dJ'_\perp, \quad (4-12)$$

where $J_\perp \equiv (J_x^2 + J_y^2)^{1/2}$. The distribution of J_z is

$$f_z(J_z) = C_z \tilde{B} \exp(-\Psi), \quad (4-13)$$

where C_z is a normalization constant determined by

$$\int_{-\infty}^{+\infty} f_z(J_z) dJ_z = 1 \quad (4-14)$$

and

$$\Psi(J_z) = \int_0^{J_z} \left[\frac{-2\tilde{A}_z}{\tilde{B}_{zz}} \right] dJ'_z. \quad (4-15)$$

The coefficients \tilde{A} and \tilde{B} are functions of J_z determined by averaging the diffusion coefficients in equation (3-8) over the transverse angular momentum components, thus:

$$\tilde{A}_z \equiv \int_{-\infty}^{+\infty} \int_{-\infty}^{+\infty} \bar{A}_z f_{xy} dJ_x dJ_y \quad (4-16)$$

and

$$\tilde{B}_{zz} \equiv \int_{-\infty}^{+\infty} \int_{-\infty}^{+\infty} \bar{B}_{zz} f_{xy} dJ_x dJ_y. \quad (4-17)$$

This completes the solution.

One can easily verify that solution (4-9) reduces to the exact analytic solution for spherical grains (PS71) in the appropriate limit. An additional check is provided by comparing R values obtained analytically from eq. (4-9) with numerical solutions of the Langevin equations for large δ_m . The results of a few tests with $\delta_m = 100$ are given in Table 7. The numerical R values were obtained by integrating the Langevin equations with $\Delta t = 10^{-5}$ and $T = 10^5$ dimensionless units.¹⁰ According to expression (4-9), the numerical and analytic

¹⁰It took 3.5 CPU days on a Sun 4 to compute each of these points.

results should agree to within $\sim 1\%$ if the discrepancies are due mainly to the accuracy of the adiabatic approximation rather than errors in the numerics. The discrepancies are 0.3–2%, consistent with this interpretation. The fact that the numerical R values are systematically *smaller* than the analytic results reinforces this conclusion.

The Rayleigh reduction factor for superparamagnetic grains depends only on a/b and T_s/T_g . Values of R can be calculated straightforwardly, in principle, from expressions (4-9) and (3-11). However this involves the numerical evaluation of certain multiple integrals and a large amount of computation. We have therefore tabulated the R values for superparamagnetic grains in Table 8.

5. Comparison with earlier work

5.1. Classical studies

The objective of this paper has been to provide accurate calculations on the Davis-Greenstein effect incorporating all physical processes now believed to be relevant. The important issue of how our calculations bear on the classical “grain alignment problem” is deferred to a future paper, where we make a comprehensive comparison between the observational constraints, our calculations on the DG effect and the calculations from forthcoming papers on other alignment mechanisms. Nevertheless, a brief comparison of the our results with previous studies of DG alignment is appropriate.

Until recently, the standard work on DG alignment was the Monte Carlo study of PS71, who described the alignment of oblate and prolate grains including gas-grain collisions, evaporation of molecules from the grain surface, magnetic dissipation, and thermal fluctuations in the grain magnetization. PS71 did not include Barnett relaxation, whose relevance to grain alignment was not appreciated until the work of P79. The nature of the Monte Carlo method used by PS71 forced them to adopt some computational expedients¹¹ but otherwise their simulations model the alignment with complete verisimilitude. Thus, the essential difference between our calculations and those of P71 is the inclusion of Barnett relaxation in the present study.

In Figure 13 we compare values of Q_X , Q_J and R obtained with our Langevin code (solid curves) and values for corresponding cases tabulated in PS71 (symbols). Not surprisingly,

¹¹For example, they modelled the grain surface with just 4 patches, scaled up the gas/grain mass ratio from a realistic value of $\sim 10^{-12}$ to “something like 10^{-2} ” and represented the Maxwellian velocity distribution of the gas particles by two delta functions.

there is good agreement on Q_J , the results from both studies being very close to the “spherical solution” for reasons discussed in §4.1. However there are large differences in the solutions for Q_X . In PS71, the motion of \mathbf{a} in the body frame is caused by gas damping. Thus, the PS71 values for Q_X are very close to the “Maxwellian solution”. We assume that the motion of \mathbf{a} is caused by Barnett relaxation. Consequently, we find perfect alignment of \mathbf{a} with \mathbf{J} for $T_s/T_g = 0$, with Q_X decreasing monotonically to the Maxwellian solution as $T_s/T_g \rightarrow 1$. The behavior of Q_X and Q_J explains why our solutions for R are systematically larger than those of PS71.¹² We conclude that the Barnett effect generally increases the efficiency of DG alignment. The enhancement is a factor of ≈ 3 for $T_s/T_g \ll 1$ but decreases rapidly as the dust temperature increases. For $T_s/T_g \gtrsim 0.3$, there is little difference between our solutions and those of PS71.

Figure 14 compares the δ_m dependence of our solutions with analogous solutions from PS71, for the case of cold grains with $T_s/T_g = 1/9$. For small δ_m , our R values exceed those of PS71 by factors of 2–3. Our results appear to converge to those of PS71 for $\delta_m \gg 1$. However, it is not clear whether the convergence occurs for other axis- and temperature ratios, there being no obvious physical explanation for this behavior.

5.2. L97

The essential difference between L97 and this paper is that the former replaces the random variables $\cos^2 \theta$ and $\cos^2 \beta$ with their mean values in the Fokker-Planck equation. The correlation between θ and β , which was neglected in earlier studies, was introduced in L97 through varying the value of $|J|$. Therefore, it would be correct to write down the assumed dependence of R on Q_J and Q_X in L97 in the following way:

$$R \approx Q_J Q_X (J | \langle \cos^2 \beta \rangle) \quad , \quad (5-1)$$

where $J | \langle \cos^2 \beta \rangle$ expresses the conditional dependence of J on β . We briefly discuss the perturbation procedure in Appendix C, as some points of it have been rectified after L97 was published. In fact, this is the first actual use of the perturbation procedure developed in L97.

To obtain R we start with the Maxwellian value of angular momentum (see LR97)

$$J_{\text{Max}}^2 = \left[1 + \frac{(a/b)^2}{2} \right] \left(1 + \frac{T_{\text{av}}}{T_s} \right) \quad (5-2)$$

¹²This would not be the case if the “correlation factor”, τ , were different in the two studies. In fact, $\tau = 0.6\text{--}0.7$ for the PS71 data plotted in Fig. 13 (see PS71, Table 2), nearly identical to our mean τ value.

corresponding to the temperature (see L95, L97):

$$T_{\text{av}} = \frac{T_m + T_s \delta_{i-1}}{1 + \delta_{i-1}} . \quad (5-3)$$

This enables us to find $\cos^2 \beta$ and $\cos^2 \theta$ that are used to iterate the mean value of angular momentum and Q_J and Q_X . We find that the iterations quickly converge and that the mean value of grain angular momentum is much more sensitive to variations of β than of θ .

The angles β and θ are correlated within the perturbative approach through the value of the grain angular momentum. If we disregard small terms proportional to powers of small parameter γ , the value of the mean angular momentum that is used within the perturbative approximation is (see (C10))

$$\langle J^2 \rangle_i \approx \frac{2kT_{\text{av}}I_{\parallel}}{(1 - \cos^2 \beta_i [1 - \aleph_i^2])(1 + \sin^2 \theta_i [h - 1])} \quad (5-4)$$

where i denotes the iteration number. It is clear from eq. (5-4) that as $\cos^2 \beta$ changes so does $\langle J^2 \rangle_i$. But according to (C4) $\langle J^2 \rangle_i$ determines the value of Q_X and therefore $\cos^2 \theta$ (see eq. (2-9)).

To calibrate the accuracy of the perturbative method, we have carried out a point-by-point comparison between the numerical R values compiled in Tables 2–6 and corresponding values obtained with the fifth-order iterative method (see Appendix C). We find that the mean error in the perturbative results is 16.8%, the sign indicating that the perturbative method (slightly) overestimates the true solution. Given the various idealizations in our grain model, this accuracy should be sufficient for many applications.

6. Future work

Does our present paper mean that the theory of Davis-Greenstein alignment is complete? We see a couple of outstanding problems that we hope to handle in the near future: The present study describes oblate grains. Although there exists some evidence that aligned grains tend to be oblate (Hildebrand 1988) a study of prolate grain alignment is needed. Our solutions assume that the magnetic properties of grains are isotropic. This is an excellent approximation for paramagnetic grains, but ferromagnetic grains should be anisotropic (see DL98). This means that for sufficiently high δ_m we have to consider the anisotropy¹³ of the grain magnetic response. Therefore a quantitative study of anisotropy effects is necessary.

¹³ In some instances, e.g., when a grain contains numerous superparamagnetic inclusions, the magnetic response can be isotropic despite high δ_m . This is probably an exception, however.

JS67 attracted the attention of researchers to the necessity of studying the magnetic response of grains. A recent study by DL98 clarified a number of issues, especially relevant to the high frequency magnetic response of candidate materials. We feel that the low frequency magnetic response deserves a similar study. We conclude that there is plenty of work to be done on Davis-Greenstein alignment. We will be lucky to finish this work by the half-century anniversary of DG51.

7. Summary

The principal results of this paper are as follows:

1. We have calculated the efficiency of the Davis-Greenstein effect for oblate spheroidal grains of arbitrary axis ratio. Our description of the grain dynamics includes gas damping, magnetic damping and Barnett relaxation.
2. We have calculated the alignment of ordinary paramagnetic grains in an “adiabatic approximation” that is accurate to $\mathcal{O}(\epsilon)$, where $\epsilon \sim 10^{-3}$ is the ratio of the timescale for Barnett relaxation to the dynamical timescale for the angular momentum.
3. For ordinary grains, we have tabulated the Rayleigh factor, R , on a grid of >1000 combinations of the relevant parameters. We have estimated the accuracy of these results using various benchmark tests. The error in R is typically a few units in the third decimal place.
4. The main difference between our paper and classical studies of DG alignment is the incorporation of Barnett relaxation in the present study. Including the Barnett effect enhances R by factors up to ≈ 3 for small dust-to-gas temperature ratios but makes little difference for $T_s/T_g > 0.3$.
5. We have calibrated the accuracy of an approximate method proposed in L97. The mean error in values of R computed via the perturbative method is $\approx 17\%$.
6. We have derived an exact analytic solution for the alignment of superparamagnetic grains. The solution is based on an adiabatic approximation that is accurate to $\mathcal{O}(\delta_m^{-1})$.
7. Our calculations on superparamagnetic grains show that DG alignment is only efficient if the grains are much colder than the gas. The commonly-held view that superparamagnetism produces “perfect” alignment under realistic conditions is a misconception.

Acknowledgments — We thank Bruce Draine for helpful discussions on various aspects of grain alignment. This work was partially supported by NASA grant NAG5-2858.

TABLE 1

Dynamical Timescales^a

Symbol	Definition	Value (s)
t_{rot}	Rotation period	$7 \times 10^{-5} \rho_{s,0}^{1/2} T_{g,1}^{-1/2} (a/b)^{1/2} b_{-5}^{5/2}$
t_{Lar}	Larmor period	$2 \times 10^5 \rho_{s,0} (\chi'_{-3})^{-1} B_{-5}^{-1} b_{-5}^2$
t_{Bar}	Barnett time	$4 \times 10^6 \rho_{s,0}^2 K_{-13}^{-1} T_{g,1}^{-1} \frac{(a/b)(1+a^2/b^2)^3}{(1-a^2/b^2)} b_{-5}^7$
t_{gas}	Gas damping time	$7 \times 10^9 \Gamma_{\parallel}^{-1} \rho_{s,0} n_4^{-1} T_{g,1}^{-1/2} (a/b) b_{-5}$
t_{mag}	Magnetic damping time	$4 \times 10^{12} \rho_{s,0} K_{-13}^{-1} B_{-5}^{-2} b_{-5}^2$

^aTimescales for a homogeneous, oblate spheroid rotating about its symmetry axis with kinetic energy $kT_g/2$ in a gas of pure H₂ (after RDGF93, Table 1). The quantity $K \equiv \chi''/\omega$ depends on the uncertain grain composition. The scaling of K is appropriate for ordinary paramagnetic substances; for superparamagnetic grains, increase K by an uncertain factor $\lesssim 10^5$ (Draine 1996).

TABLE 2
Rayleigh Reduction factor for $a/b = 0.1$

$\log \delta_m$	T_s/T_g								
	0	.1	.2	.3	.4	.5	.6	.7	.8
-1.00	0.018	0.014	0.008	0.006	—	—	—	—	—
-0.90	0.022	0.014	0.010	0.006	—	—	—	—	—
-0.80	0.030	0.019	0.011	0.008	0.005	—	—	—	—
-0.70	0.035	0.023	0.015	0.009	0.006	—	—	—	—
-0.60	0.046	0.029	0.018	0.011	0.007	0.005	—	—	—
-0.50	0.055	0.035	0.021	0.014	0.009	0.006	—	—	—
-0.40	0.066	0.040	0.025	0.016	0.011	0.007	0.005	—	—
-0.30	0.083	0.049	0.029	0.019	0.012	0.009	0.006	—	—
-0.20	0.101	0.059	0.034	0.022	0.014	0.010	0.006	—	—
-0.10	0.119	0.068	0.039	0.025	0.016	0.011	0.008	0.005	—
0	0.142	0.078	0.045	0.027	0.019	0.013	0.008	0.005	—
0.10	0.169	0.090	0.050	0.032	0.021	0.013	0.009	0.006	—
0.20	0.200	0.101	0.056	0.035	0.022	0.015	0.010	0.007	—
0.30	0.228	0.112	0.061	0.038	0.025	0.017	0.011	0.007	—
0.40	0.263	0.121	0.066	0.041	0.026	0.017	0.012	0.008	—
0.50	0.300	0.133	0.070	0.043	0.028	0.018	0.013	0.008	0.005
0.60	0.337	0.140	0.074	0.045	0.029	0.020	0.013	0.008	0.005
0.70	0.372	0.149	0.078	0.047	0.030	0.020	0.013	0.009	0.005
0.80	0.411	0.154	0.081	0.050	0.032	0.021	0.014	0.009	0.005
0.90	0.452	0.161	0.082	0.050	0.032	0.022	0.014	0.009	0.005
1.00	0.490	0.167	0.086	0.051	0.033	0.022	0.015	0.009	0.005
1.10	0.527	0.170	0.087	0.052	0.034	0.022	0.015	0.009	0.005
1.20	0.562	0.175	0.088	0.053	0.034	0.022	0.015	0.009	0.005
1.30	0.597	0.176	0.089	0.054	0.034	0.023	0.015	0.009	0.005
1.40	0.629	0.179	0.090	0.054	0.034	0.023	0.015	0.009	0.005
1.50	0.661	0.178	0.089	0.054	0.034	0.023	0.014	0.009	0.005

TABLE 3
Rayleigh Reduction factor for $a/b = 0.3$

$\log \delta_m$	T_s/T_g								
	0	.1	.2	.3	.4	.5	.6	.7	.8
-1.00	0.015	0.011	0.007	—	—	—	—	—	—
-0.90	0.021	0.015	0.009	0.006	—	—	—	—	—
-0.80	0.026	0.018	0.011	0.007	0.005	—	—	—	—
-0.70	0.031	0.021	0.013	0.008	0.006	—	—	—	—
-0.60	0.042	0.026	0.016	0.011	0.007	—	—	—	—
-0.50	0.053	0.033	0.019	0.012	0.008	0.005	—	—	—
-0.40	0.064	0.039	0.023	0.015	0.009	0.006	—	—	—
-0.30	0.079	0.046	0.027	0.018	0.012	0.008	0.005	—	—
-0.20	0.098	0.056	0.032	0.020	0.013	0.009	0.006	—	—
-0.10	0.120	0.064	0.036	0.023	0.015	0.010	0.007	—	—
0	0.140	0.074	0.042	0.026	0.017	0.011	0.008	0.005	—
0.10	0.167	0.083	0.046	0.028	0.019	0.012	0.008	0.006	—
0.20	0.197	0.094	0.051	0.032	0.020	0.014	0.009	0.005	—
0.30	0.230	0.102	0.055	0.034	0.022	0.015	0.010	0.006	—
0.40	0.260	0.113	0.059	0.036	0.024	0.015	0.010	0.007	—
0.50	0.296	0.120	0.064	0.039	0.025	0.016	0.011	0.007	—
0.60	0.336	0.128	0.066	0.040	0.026	0.018	0.012	0.007	—
0.70	0.375	0.136	0.070	0.042	0.028	0.018	0.012	0.008	—
0.80	0.412	0.141	0.073	0.043	0.028	0.019	0.013	0.007	0.005
0.90	0.451	0.148	0.074	0.044	0.029	0.019	0.013	0.008	0.005
1.00	0.490	0.151	0.076	0.046	0.029	0.020	0.013	0.008	0.005
1.10	0.526	0.154	0.078	0.046	0.030	0.020	0.013	0.008	0.005
1.20	0.562	0.155	0.077	0.046	0.029	0.020	0.013	0.008	0.005
1.30	0.600	0.159	0.080	0.047	0.030	0.020	0.013	0.008	0.005
1.40	0.629	0.161	0.079	0.047	0.031	0.020	0.013	0.008	0.005
1.50	0.663	0.161	0.081	0.047	0.030	0.020	0.013	0.008	—

TABLE 4
Rayleigh Reduction factor for $a/b = 0.5$

$\log \delta_m$	0	.1	.2	.3	.4	.5	.6	.7
-1.00	0.014	0.010	0.005	—	—	—	—	—
-0.90	0.017	0.012	0.007	0.005	—	—	—	—
-0.80	0.022	0.015	0.009	0.005	—	—	—	—
-0.70	0.032	0.020	0.011	0.007	0.005	—	—	—
-0.60	0.039	0.024	0.013	0.008	0.006	—	—	—
-0.50	0.049	0.029	0.016	0.010	0.007	0.005	—	—
-0.40	0.064	0.035	0.019	0.012	0.008	0.005	—	—
-0.30	0.079	0.041	0.022	0.014	0.009	0.006	—	—
-0.20	0.095	0.048	0.026	0.016	0.010	0.007	0.005	—
-0.10	0.115	0.056	0.031	0.018	0.012	0.008	0.005	—
0	0.139	0.064	0.034	0.021	0.013	0.009	0.006	—
0.10	0.167	0.072	0.037	0.023	0.015	0.010	0.006	—
0.20	0.195	0.079	0.041	0.025	0.016	0.011	0.007	—
0.30	0.228	0.088	0.044	0.026	0.017	0.011	0.008	0.005
0.40	0.262	0.096	0.047	0.028	0.018	0.012	0.008	0.005
0.50	0.298	0.101	0.051	0.030	0.019	0.013	0.009	0.006
0.60	0.335	0.105	0.052	0.032	0.021	0.013	0.009	0.006
0.70	0.371	0.111	0.055	0.032	0.020	0.014	0.009	0.006
0.80	0.409	0.116	0.056	0.034	0.022	0.015	0.009	0.006
0.90	0.453	0.120	0.059	0.034	0.022	0.015	0.010	0.006
1.00	0.492	0.124	0.060	0.035	0.022	0.015	0.010	0.006
1.10	0.527	0.126	0.061	0.035	0.023	0.015	0.010	0.006
1.20	0.564	0.127	0.062	0.036	0.023	0.015	0.010	0.006
1.30	0.598	0.129	0.062	0.037	0.023	0.015	0.010	0.006
1.40	0.631	0.131	0.062	0.036	0.023	0.016	0.010	0.006
1.50	0.663	0.131	0.063	0.037	0.024	0.015	0.010	0.006

TABLE 5
Rayleigh Reduction factor for $a/b = 0.7$

$\log \delta_m$	T_s/T_g						
	0	.1	.2	.3	.4	.5	.6
-1.00	0.013	0.007	—	—	—	—	—
-0.90	0.020	0.008	0.005	—	—	—	—
-0.80	0.027	0.012	0.006	—	—	—	—
-0.70	0.032	0.015	0.007	—	—	—	—
-0.60	0.042	0.018	0.009	0.005	—	—	—
-0.50	0.053	0.020	0.011	0.006	—	—	—
-0.40	0.064	0.025	0.012	0.007	0.005	—	—
-0.30	0.080	0.030	0.015	0.008	0.005	—	—
-0.20	0.096	0.035	0.017	0.010	0.006	—	—
-0.10	0.118	0.039	0.020	0.012	0.007	0.005	—
0	0.141	0.046	0.021	0.012	0.008	0.005	—
0.10	0.167	0.050	0.024	0.014	0.009	0.006	—
0.20	0.195	0.056	0.027	0.015	0.010	0.007	0.005
0.30	0.227	0.063	0.029	0.017	0.011	0.007	0.005
0.40	0.261	0.066	0.030	0.018	0.011	0.008	0.005
0.50	0.296	0.071	0.032	0.019	0.012	0.008	0.005
0.60	0.335	0.073	0.033	0.020	0.013	0.008	0.006
0.70	0.376	0.077	0.035	0.020	0.013	0.009	0.006
0.80	0.413	0.079	0.036	0.021	0.013	0.009	0.006
0.90	0.451	0.082	0.037	0.021	0.014	0.009	0.006
1.00	0.490	0.083	0.038	0.022	0.014	0.009	0.006
1.10	0.528	0.084	0.039	0.022	0.014	0.009	0.006
1.20	0.563	0.085	0.039	0.022	0.015	0.009	0.006
1.30	0.598	0.087	0.039	0.023	0.015	0.010	0.006
1.40	0.630	0.088	0.040	0.023	0.015	0.010	0.006
1.50	0.663	0.088	0.040	0.023	0.015	0.010	0.006

TABLE 6
Rayleigh reduction factor for $a/b = 0.9$

$\log \delta_m$	T_s/T_g				
	0	.1	.2	.3	.4
-1.00	0.015	—	—	—	—
-0.90	0.021	—	—	—	—
-0.80	0.026	—	—	—	—
-0.70	0.035	0.005	—	—	—
-0.60	0.042	0.007	—	—	—
-0.50	0.056	0.008	—	—	—
-0.40	0.068	0.009	—	—	—
-0.30	0.082	0.011	0.005	—	—
-0.20	0.100	0.013	0.006	—	—
-0.10	0.119	0.015	0.006	—	—
0	0.141	0.016	0.007	—	—
0.10	0.169	0.018	0.008	0.005	—
0.20	0.198	0.020	0.009	0.005	—
0.30	0.227	0.022	0.010	0.005	—
0.40	0.261	0.023	0.010	0.006	—
0.50	0.300	0.024	0.011	0.006	—
0.60	0.335	0.025	0.011	0.006	—
0.70	0.372	0.026	0.012	0.007	—
0.80	0.414	0.027	0.012	0.007	—
0.90	0.450	0.028	0.012	0.007	0.005
1.00	0.489	0.029	0.013	0.007	0.005
1.10	0.526	0.029	0.013	0.007	0.005
1.20	0.563	0.030	0.013	0.007	0.005
1.30	0.598	0.030	0.013	0.007	0.005
1.40	0.631	0.030	0.013	0.008	0.005
1.50	0.661	0.030	0.013	0.008	0.005

TABLE 7
 Analytic Solution for Superparamagnetic Grains
 vs. Numerical Solution for $\delta_m = 100$

a/b	T_s/T_g	Analytic	Numerical
0.1	0.1	0.1887	0.1857
0.1	0.2	0.0951	0.0940
0.1	0.3	0.0571	0.0559
0.1	0.4	0.0370	0.0366
0.5	0.1	0.1369	0.1353
0.5	0.3	0.0388	0.0380
0.5	0.5	0.0166	0.0165

TABLE 8
 Rayleigh reduction factor for superparamagnetic grains

a/b	T_s/T_g									
	.1	.2	.3	.4	.5	.6	.7	.8	.9	
0.1	.1887	.0951	.0571	.0370	.0247	.0164	.0106	.0061	.0027	
0.3	.1688	.0839	.0502	.0324	.0217	.0144	.0093	.0054	.0024	
0.5	.1369	.0657	.0388	.0250	.0166	.0111	.0071	.0041	.0018	
0.7	.0916	.0417	.0242	.0155	.0103	.0068	.0044	.0025	.0011	
0.9	.0316	.0138	.0080	.0051	.0034	.0023	.0014	.0008	.0004	

REFERENCES

Bradley J.P., 1994, *Science*, 265, 925

Davis L., Jr, Greenstein J.L., 1951, *ApJ*, 114, 206 (DG51)

Draine B.T., 1996, in Roberge W.G., Whittet D.C.B., eds, *ASP Conf. Ser. Vol. 97, Polarimetry of the Interstellar Medium*. Astron. Soc. Pac., San Francisco, p. 16

Draine B.T., Lazarian A., 1998, *astro-ph* 9807009 (DL98)

Goodman A.A., Whittet D.C.B., 1995, *ApJ*, 455, L181

Hildebrand R.H., 1988, *QJRAS*, 29, 327

—. 1996, in Roberge W.G., Whittet D.C.B., eds, *ASP Conf. Ser. Vol. 97, Polarimetry of the Interstellar Medium*. Astron. Soc. Pac., San Francisco, p. 254

Jones R.V., Spitzer, L., Jr, 1967, *ApJ*, 147, 943 (JS67)

Lazarian A., 1994, *MNRAS*, 268, 713 (L94)

Lazarian A., 1995, *ApJ*, 453, 229 (L95)

Lazarian A., 1997, *MNRAS*, 288, 609 (L97)

Lazarian A., 1998, *MNRAS*, 293, 208

Lazarian A., Efroimsky, M. 1999, preprint

Lazarian A., Roberge W.G., 1997, *ApJ*, 484, 230 (LR97)

Lee H.M., Draine B.T., 1985, *ApJ*, 290, 211

Martin P.G., 1974, *ApJ*, 187, 461

Martin P.G., 1995, *ApJ*, 445, L63

Mathis J.S., 1986, *ApJ*, 308, 281

Purcell E.M., 1969, *Physica*, 41, 100

—. 1979, *ApJ*, 231, 404 (P79)

Purcell E.M., Spitzer, L., Jr, 1971, *ApJ*, 167, 31 (PS71)

Risken H. 1984, *The Fokker-Planck Equation*, Springer-Verlag, 1984

Roberge W.G., 1997, MNRAS, 291, 345 (R97)

Roberge W.G., DeGraff T.A., Flaherty J.E., 1993 ApJ, 418, 287 (RDGF93)

Spitzer, L., Jr, Tukey, J.W., 1951, ApJ, 114, 187

Wolff M.J., Clayton G.C., Kim S.-H., Martin P.G., Anderson C.M., 1997, ApJ, 478, 395

A. Diffusion coefficients in equation (3-1)

A.1. Gas damping

The diffusion coefficients for gas damping were derived elsewhere (LR97; L97). The (dimensionless) mean torque has body frame components

$$A_{g,x}^b = -h \left(\Gamma_{\perp}/\Gamma_{\parallel} \right) J_x^b, \quad (\text{A1})$$

$$A_{g,y}^b = -h \left(\Gamma_{\perp}/\Gamma_{\parallel} \right) J_y^b, \quad (\text{A2})$$

and

$$A_{g,z}^b = -J_z^b. \quad (\text{A3})$$

The diffusion tensor is diagonal in the body frame with

$$B_{g,xx}^b = \left(\Gamma_{\perp}/\Gamma_{\parallel} \right) (1 + T_s/T_g), \quad (\text{A4})$$

$$B_{g,yy}^b = B_{g,xx}^b, \quad (\text{A5})$$

and

$$B_{g,zz}^b = (1 + T_s/T_g). \quad (\text{A6})$$

The dimensionless shape factors

$$\Gamma_{\parallel}(e) = \frac{3}{16} \left\{ 3 + 4(1 - e^2)g(e) - e^{-2} \left[1 - (1 - e^2)^2 g(e) \right] \right\} \quad (\text{A7})$$

and

$$\Gamma_{\perp}(e) = \frac{3}{32} \left\{ 7 - e^2 + (1 - e^2)^2 g(e) + (1 - 2e^2) \left[1 + e^{-2} \left[1 - (1 - e^2)^2 g(e) \right] \right] \right\}, \quad (\text{A8})$$

are weak functions of the eccentricity, $e \equiv \sqrt{1 - a^2/b^2}$, with

$$g(e) \equiv \frac{1}{2e} \ln \left(\frac{1+e}{1-e} \right). \quad (\text{A9})$$

The diffusion coefficients in equation (3-1) are evaluated in the inertial frame. To obtain these coefficients from expressions (A1)–(A6) we (i) transform components from the body frame to the inertial frame; and (ii) average the resulting expressions over the rapidly-changing angles ϕ and ψ (see L97). The calculations are straightforward but tedious and here we simply give the results. The mean torque has inertial frame components

$$A_{g,i} = - \left(1 + \lambda \sin^2 \theta \right) J_i \quad i = x, y, z, \quad (\text{A10})$$

where

$$\lambda \equiv h \left(\Gamma_{\perp}/\Gamma_{\parallel} \right) - 1. \quad (\text{A11})$$

The diffusion tensor has inertial frame components

$$B_{g,xx} = \frac{1}{2} (1 + T_s/T_g) \left[(1 + \cos^2 \beta) P_1 + \sin^2 \beta P_2 \right], \quad (\text{A12})$$

$$B_{g,yy} = B_{g,xx}, \quad (\text{A13})$$

and

$$B_{g,zz} = (1 + T_s/T_g) \left[\sin^2 \beta P_1 + \cos^2 \beta P_2 \right], \quad (\text{A14})$$

where

$$P_1 \equiv 1 - \gamma \left(1 - \sin^2 \theta/2 \right) \quad (\text{A15})$$

and

$$P_2 \equiv \left(1 - \gamma \sin^2 \theta \right) \quad (\text{A16})$$

are functions of θ and

$$\gamma \equiv 1 - \Gamma_{\perp}/\Gamma_{\parallel}. \quad (\text{A17})$$

A.2. Magnetic damping

The mean torque was derived by DG51 (see DG51, eq. [81]). In dimensionless units, the inertial frame components are

$$A_{m,x} = -Z(\theta) \delta_m J_x, \quad (\text{A18})$$

$$A_{m,y} = -Z(\theta) \delta_m J_y, \quad (\text{A19})$$

and

$$A_{m,z} = 0, \quad (\text{A20})$$

where

$$Z(\theta) \equiv \left[1 + (h - 1) \sin^2 \theta \right]. \quad (\text{A21})$$

The diffusion tensor for paramagnetic relaxation in spheroidal grains does not appear in previous papers on the DG effect, which either ignored thermal fluctuations (e.g., DG51) or used the diffusion tensor for spheres (JS67). However the diffusion tensor is uniquely determined by the principle of detailed balance, which requires the probability current at

each point in phase space to vanish in thermodynamic equilibrium. Setting the current along the x direction to zero yields

$$A_{m,x} f^* - \frac{1}{2} \frac{\partial}{\partial J_x} (B_{m,xx} f^*) = 0, \quad (A22)$$

where

$$f^* = C \exp \left(\frac{Z J^2}{2 T_s / T_g} \right) \quad (A23)$$

is the thermal equilibrium distribution of the dimensionless angular momentum and C is a normalization constant. Consistent with the symmetry of the problem, we have assumed that the off-diagonal components of the diffusion tensor are zero. The unique solution of eq. (A23) with $B_{m,xx}$ finite for all J_x is

$$B_{m,xx} = 2 (T_s / T_g) \delta_m. \quad (A24)$$

The analogous conditions for the y and z directions yield

$$B_{m,yy} = B_{m,xx} \quad (A25)$$

and

$$B_{m,zz} = 0. \quad (A26)$$

B. Analytic solution for superparamagnetic grains

B.1. Adiabatic elimination

We seek an approximate solution to equation (3-8) of the form

$$f_{\text{ext}}(J_x, J_y, J_z) = f_{xy}(J_x, J_y|J_z) f_z(J_z) \quad (\text{B1})$$

subject to the normalization conditions

$$\int_{-\infty}^{+\infty} \int_{-\infty}^{+\infty} f_{xy}(J_x, J_y|J_z) dJ_x dJ_y = 1 \quad (\text{B2})$$

and

$$\int_{-\infty}^{+\infty} f_z(J_z) dJ_z = 1. \quad (\text{B3})$$

We require our approximation to be accurate to $\mathcal{O}(\delta_m^{-1})$. This means that we may neglect the terms of order unity in comparison with the terms of order δ_m in expressions (3-12)–(3-14) and (3-19)–(3-21) for the diffusion coefficients. For the linear coefficients, this gives

$$\bar{A}_x \approx -[1 + (h-1)\sigma] J_x \delta_m \equiv \tilde{A}_x \delta_m, \quad (\text{B4})$$

$$\bar{A}_y \approx -[1 + (h-1)\sigma] J_y \delta_m \equiv \tilde{A}_y \delta_m, \quad (\text{B5})$$

and

$$\bar{A}_z = -(1 + \lambda\sigma) J_z. \quad (\text{B6})$$

The analogous approximations for the quadratic diffusion coefficients are

$$\bar{B}_{xx} \approx 2(T_s/T_g) \delta_m \equiv \tilde{B}_{xx} \delta_m, \quad (\text{B7})$$

$$\bar{B}_{yy} \approx \tilde{B}_{xx} \delta_m, \quad (\text{B8})$$

and

$$\bar{B}_{zz} = (1 + T_s/T_g) [\sin^2 \beta P_1(J) + \cos^2 \beta P_2(J)], \quad (\text{B9})$$

where $P_1(J)$ and $P_2(J)$ are defined in eqs. (A15) and (A16). The physical content of our approximation is that the torques perpendicular to \mathbf{B} are provided entirely by magnetic dissipation; evidently this is accurate to order $t_{\text{mag}}/t_{\text{gas}}$.

To proceed, we substitute expressions (B1), (B4)–(B6) and (B7)–(B9) into equation (3-8). After a little algebra, the latter becomes

$$f_z \mathcal{L}_{xy} f_{xy} + \delta_m^{-1} \mathcal{L}_z f_{xy} f_z = 0, \quad (\text{B10})$$

where

$$\mathcal{L}_{xy} \equiv -\frac{\partial}{\partial J_x} \tilde{A}_x \cdot -\frac{\partial}{\partial J_y} \tilde{A}_y \cdot + \frac{1}{2} \frac{\partial^2}{\partial J_x^2} \tilde{B}_{xx} \cdot + \frac{1}{2} \frac{\partial^2}{\partial J_y^2} \tilde{B}_{yy} \cdot \quad (\text{B11})$$

and

$$\mathcal{L}_z \equiv -\frac{\partial}{\partial J_z} \bar{A}_z \cdot + \frac{1}{2} \frac{\partial^2}{\partial J_z^2} \bar{B}_{zz} \cdot \quad (\text{B12})$$

B.2. Solution for f_{xy}

Neglecting the term of order δ_m^{-1} in equation (B10) gives

$$\mathcal{L}_{xy} f_{xy} = 0, \quad (\text{B13})$$

which is a Fokker-Planck equation for f_{xy} . After transforming¹⁴ to polar coordinates

$$J_\perp \equiv (J_x^2 + J_y^2)^{1/2} \quad (\text{B14})$$

and

$$\phi \equiv \tan^{-1} (J_y/J_x), \quad (\text{B15})$$

equation (B13) becomes

$$-\frac{\partial}{\partial J_\perp} \left[A_\perp f_\perp - \frac{1}{2} \tilde{B}_{xx} \frac{\partial f_\perp}{\partial J_\perp} \right] - \frac{\partial}{\partial \phi} \left[-\frac{1}{2} \left(\tilde{B}_{xx}/J_\perp^2 \right) \frac{\partial f_\perp}{\partial \phi} \right] = 0, \quad (\text{B16})$$

where

$$f_\perp \equiv J_\perp f_{xy} \quad (\text{B17})$$

and

$$A_\perp \equiv -[1 + (h-1)\sigma] J_\perp + \frac{\tilde{B}_{xx}}{2J_\perp}. \quad (\text{B18})$$

Equation (B16) will be satisfied if we assume that f_\perp is independent of ϕ , consistent with the symmetry of the problem, and require

$$A_\perp f_\perp - \frac{1}{2} \tilde{B}_{xx} \frac{df_\perp}{dJ_\perp} = 0. \quad (\text{B19})$$

Equation (B19) states that there is no probability current perpendicular to the \mathbf{B} direction in equilibrium (“zero-current solution” for f_\perp).

¹⁴The transformation is straightforward but tedious and only the relevant results are given here. For details, see any text on statistical mechanics (e.g., Risken 1984).

Solving eq. (B19) for f_{\perp} and using eq. (B17), we find

$$f_{xy} = C_x \exp(-\Phi), \quad (B20)$$

where C_x is determined by eq. (B2) and

$$\Phi(J_x, J_y | J_z) \equiv \left(\frac{T_g}{T_s} \right) \int_0^{J_{\perp}} [1 + (h-1)\sigma(J')] dJ'_{\perp}. \quad (B21)$$

Since \mathcal{L}_{xy} does not involve differentiation with respect to J_z , the latter appears¹⁵ only as a parameter in the solution for f_{xy} . In physical terms, this means that the distribution of J_x and J_y relaxes rapidly (“adiabatically”) to the equilibrium distribution that would obtain if J_z were frozen at its instantaneous value. Of course, this is appropriate when $t_{\text{mag}} \ll t_{\text{gas}}$.

B.3. Solution for f_z

Given the solution for f_{xy} from the preceding section, one can find f_z by setting the term $\mathcal{O}(\delta_m^{-1})$ in equation (B10) to zero. When eq. (B12) is used to expand \mathcal{L}_z in terms of derivatives, this statement becomes

$$-\frac{\partial}{\partial J_z} [\bar{A}_z f_{xy} f_z] + \frac{1}{2} \frac{\partial^2}{\partial J_z^2} [\bar{B}_{zz} f_{xy} f_z] = 0. \quad (B22)$$

If the last equation is multiplied by $dJ_x dJ_y$ and the resulting expression is integrated over all J_x and J_y , the result is

$$-\frac{d}{dJ_z} \left[\tilde{A}_z f_z - \frac{1}{2} \frac{d}{dJ_z} (\tilde{B}_{zz} f_z) \right] = 0, \quad (B23)$$

where

$$\tilde{A}_z \equiv \int_{-\infty}^{+\infty} \int_{-\infty}^{+\infty} \bar{A}_z f_{xy} dJ_x dJ_y, \quad (B24)$$

and

$$\tilde{B}_{zz} \equiv \int_{-\infty}^{+\infty} \int_{-\infty}^{+\infty} \bar{B}_{zz} f_{xy} dJ_x dJ_y. \quad (B25)$$

Equations (B23)–(B25) say that f_z satisfies a one-variable Fokker-Planck equation wherein the diffusion coefficients \bar{A} and \bar{B} have been averaged over J_x and J_y in the obvious way. The preceding discussion shows that this procedure is accurate to $\mathcal{O}(\delta_m^{-1})$.

¹⁵Recall that σ depends on J^2 , hence J_z .

The zero-current solution for f_z is elementary:

$$f_z = C_z \tilde{B}_{zz}^{-1} \exp(-\Psi), \quad (\text{B26})$$

where

$$\Psi \equiv \int_0^{J_z} \left(\frac{-2\tilde{A}_z}{\tilde{B}_{zz}} \right) dJ'_z. \quad (\text{B27})$$

This completes the solution.

C. Perturbative scheme

It was shown in L97 (see also Errata in Lazarian 1998) that calculations of $\langle Q_J \rangle$ can be performed perturbatively with

$$\langle Q_{Ji} \rangle \approx \frac{3}{2} \langle \cos^2 \beta_i \rangle - \frac{1}{2} \quad , \quad (\text{C1})$$

where

$$\langle \cos^2 \beta_{i+1} \rangle = \frac{1}{1 - \aleph_{i+1}^2} \left[1 - \frac{\aleph_{i+1}}{\sqrt{1 - \aleph_{i+1}^2}} \arcsin \sqrt{1 - \aleph_{i+1}^2} \right] \quad , \quad (\text{C2})$$

$$\aleph_i = \frac{T_{\text{av}}}{T_{\text{m}}} + \frac{\gamma}{1 + \delta_{\text{m}}} Q_{Xi} Q_{Ji} \quad , \quad (\text{C3})$$

T_{av} is given by (5-3) and T_{m} is the mean rotational temperature of grain in the absence of paramagnetic relaxation. For the sake of simplicity this temperature is frequently chosen to be equal $0.5(T_s + T_g)$, but such a choice is uncertain (see Purcell 1979).

The internal alignment measure Q_{Xi} can be found as (LR97, L97)

$$Q_{Xi} = \frac{3}{2} \left(\frac{\int_0^\pi \cos^2 \theta \sin \theta f(\theta) d\theta}{\int_0^\pi \sin \theta f(\theta) d\theta} - \frac{1}{3} \right) \quad , \quad (\text{C4})$$

$$f(\theta) = \text{const} \times \sin \theta \exp \left[-E_{\text{rot}}^{(i)}(\theta) / kT_s \right] \quad , \quad (\text{C5})$$

and

$$E_{\text{rot}}^{(i)}(\theta) = \frac{\langle J^2 \rangle_i}{2I_z} \left[1 + (h-1) \sin^2 \theta \right] \quad , \quad (\text{C6})$$

where $\langle J^2 \rangle_i$ is to be found using the distribution function for the i -th iteration is

$$f = f_{x_0} f_{y_0} f_{z_0} \approx \text{const} \times \exp(-\alpha J^2) \quad (\text{C7})$$

where

$$\alpha = \frac{(1 + \sin^2 \theta_i [h\Gamma_\perp/\Gamma_\parallel - 1])}{2kT_{\text{av}}I_\parallel} \frac{J^2 (1 - \cos^2 \beta_i [1 - \aleph_i^2])}{1} - \gamma \frac{\eta_2(\beta_i, \theta_i)T_{\text{m}}}{T_{\text{m}} + T_{\text{s}}\delta_{\text{m}}} \quad , \quad (\text{C8})$$

$$\eta_2(\beta_i, \theta_i) = \frac{1}{2} \left[\frac{1}{2} (1 + \cos^2 \theta) (1 + \cos^2 \beta) + \sin^2 \beta \sin^2 \theta \right] \quad . \quad (\text{C9})$$

In the perturbative approach all the values obtained at the i stage are treated as constants and therefore integration provides

$$\langle J \rangle_i = \text{const} \times \int_0^\infty J^2 \exp(\alpha J) J dJ = \frac{1}{2\alpha} \quad (\text{C10})$$

FIGURE CAPTIONS

Fig. 1 — Definition of the body frame, $\{\hat{\mathbf{x}}^b, \hat{\mathbf{y}}^b, \hat{\mathbf{z}}^b\}$, with $\hat{\mathbf{z}}^b$ parallel to the symmetry axis, \mathbf{a} , and the remaining basis vectors oriented arbitrarily in the equatorial plane of the grain surface (the lightly-shaded disk). The orientation of \mathbf{a} with respect to the angular momentum, \mathbf{J} , is specified by angles θ and ψ . The “ J frame” basis, $\{\hat{\mathbf{x}}^J, \hat{\mathbf{y}}^J, \hat{\mathbf{z}}^J\}$, is used only to carry out transformations between the body and inertial frames (see Fig. 2).

Fig. 2 — Definition of the inertial frame, $\{\hat{\mathbf{x}}, \hat{\mathbf{y}}, \hat{\mathbf{z}}\}$, with $\hat{\mathbf{z}}$ parallel to the interstellar magnetic field, \mathbf{B} , and the other basis vectors oriented arbitrarily in the plane perpendicular to \mathbf{B} . Angles β and ϕ specify the orientation of \mathbf{J} with respect to \mathbf{B} .

Fig. 3 — The cross sections for polarized light are defined with respect to the observer frame basis [see eqs. (2-5) and (2-6)], with $\hat{\mathbf{z}}^o$ the direction of propagation and $\hat{\mathbf{y}}^o$ along the projection of \mathbf{B} onto the plane of the sky.

Fig. 4 — In the adiabatic approximation, statistics of the θ distribution depend only on ξ^2 [a dimensionless function of J^2 , see eq. (3-4)], the grain shape and the dust-to-gas temperature ratio. Shown here are the mean values of $\cos^2 \theta$ (short dash), $\sin^2 \theta$ (long dash), and q_X (solid).

Fig. 5 — The angular momentum diffusion coefficients, and hence the Rayleigh reduction factor, depend on the grain shape. For a homogeneous grain, the dependence is only via the functions of a/b shown here: λ (short dash), γ (long dash), and $h - 1$ (solid).

Fig. 6 — Histogram: distribution of the errors in Q_J , computed by comparing the results of 100 identical numerical trials with exact solution for spherical grains (see §4.1). The mean and rms errors in Q_J are -1.5×10^{-4} and 1.2×10^{-3} , respectively. Dashed curve: Gaussian distribution with the same mean and standard deviation as the histogram.

Fig. 7 — Comparison between Q_J values computed numerically (open circles) and the predictions of the perturbative approach described in Appendix C. The calculations shown here are for the case $T_s/T_g = 0$, $a/b = 2/3$.

Fig. 8 — Similar to Fig. 6 but showing the errors in Q_X for a special case, $T_s/T_g = 1$, where an exact solution for Q_X exists (see §4.1). The mean and rms errors in Q_X are -5×10^{-4} and 5×10^{-4} , respectively.

Fig. 9 — (a) Solid curves: values of R (top), Q_J (middle) and Q_X (bottom) determined by numerical integration of the Langevin equations, plotted vs. the axis ratio. Values of the dust-to-gas temperature ratio and magnetic damping parameter are indicated. Dashed curves: product of $Q_X Q_J$ from the numerical calculations (top), the exact value of Q_J for

a spherical grain with the same T_s/T_g and δ_m (middle) and the exact value of Q_X for a Maxwellian angular momentum distribution in the grain frame (bottom). (b) Similar to (a) but for $\delta_m = 10$.

Fig. 10 — Similar to Figure 9 but showing the dependence on the magnetic damping parameter with a/b and T_s/T_g fixed.

Fig. 11 — Similar to Figure 9 but showing the dependence on the dust-to-gas temperature ratio with a/b and δ_m fixed.

Fig. 12 — Dependence of the correlation function [see eq. (4-6)] on the magnetic damping parameter. Solid curve: numerical calculations with the other parameters fixed at the indicated values. Dashed curve: approximation to ρ obtained by replacing the angular momentum distribution with the angular momentum distribution for spheres with the same T_s/T_g and δ_m (see text).

Fig. 13 — Comparison between the results of PS71 (filled circles) and our numerical results (solid). The dotted curves depict Q_J for spherical grains with the same δ_m and T_s/T_g (middle panel) and Q_X for a Maxwellian angular momentum distribution in the body frame (bottom panel).

Fig. 14 — Similar to Fig. 13 but showing the dependence on δ_m .

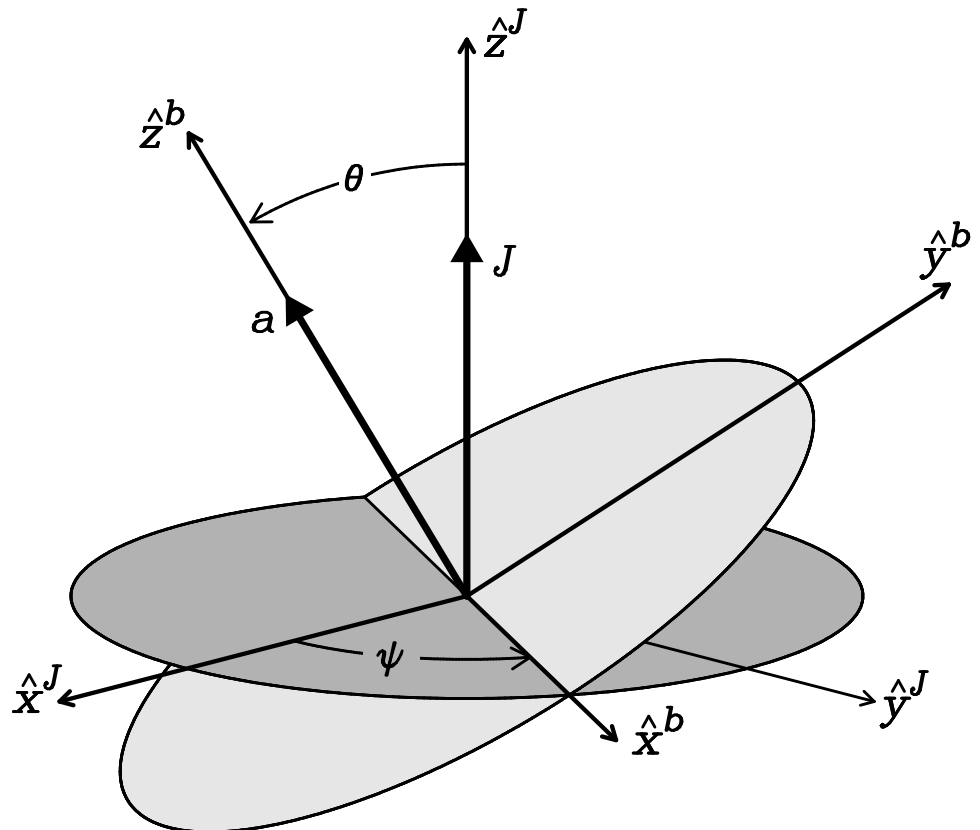


Figure 1

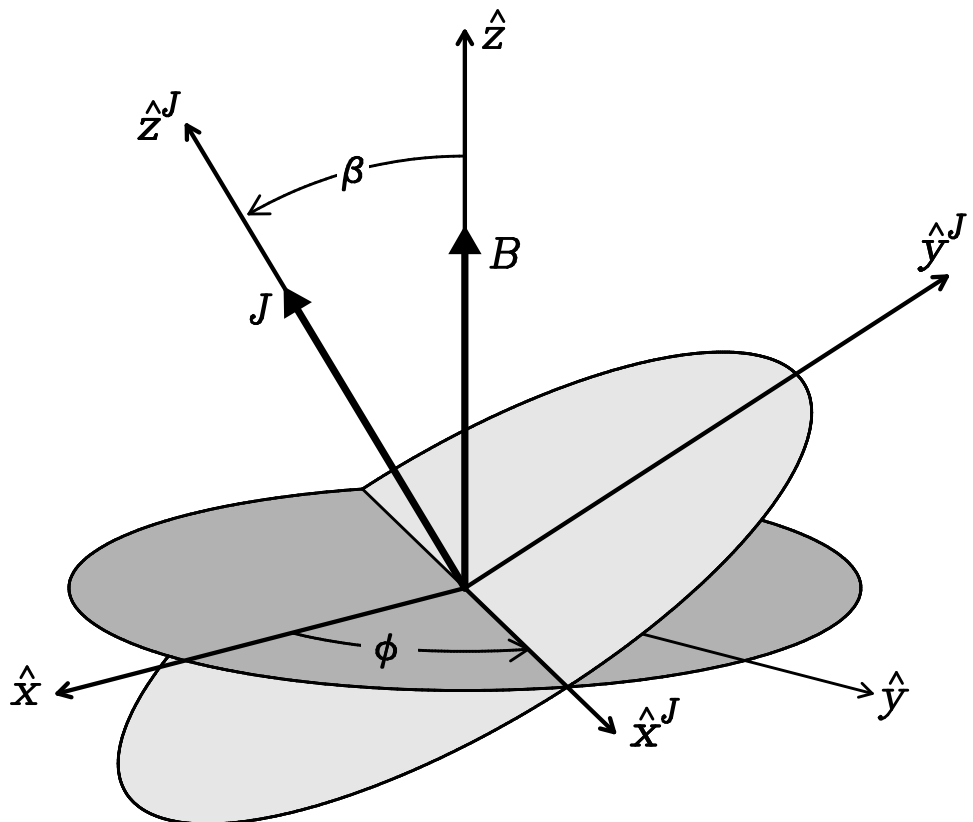


Figure 2

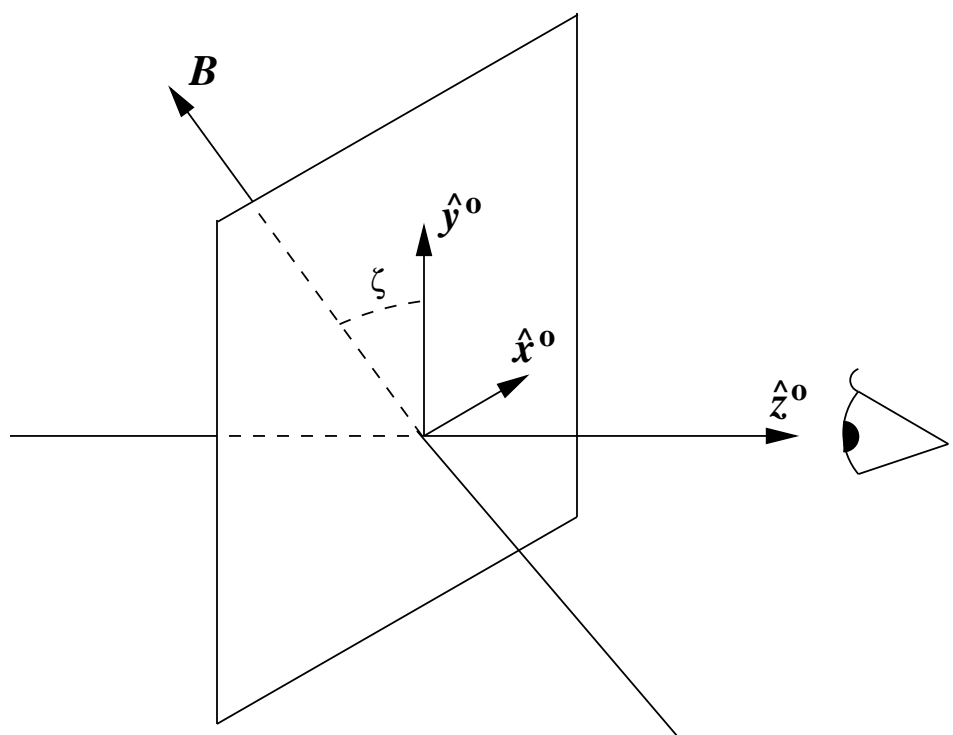


Figure 3

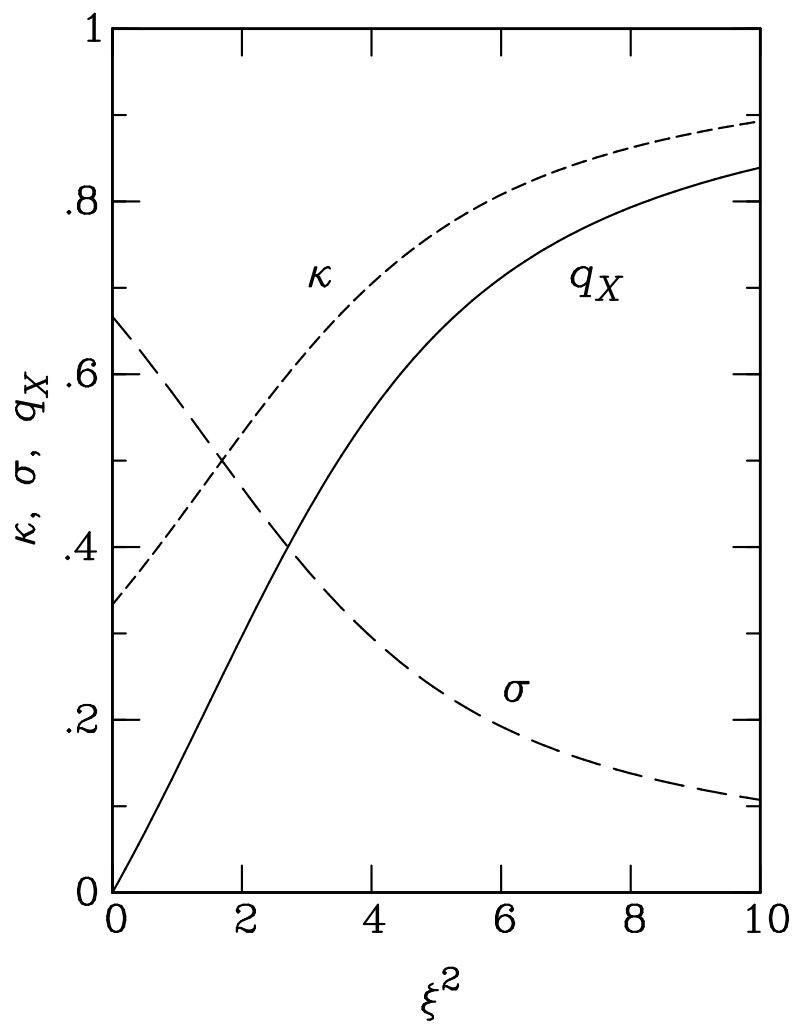


Figure 4

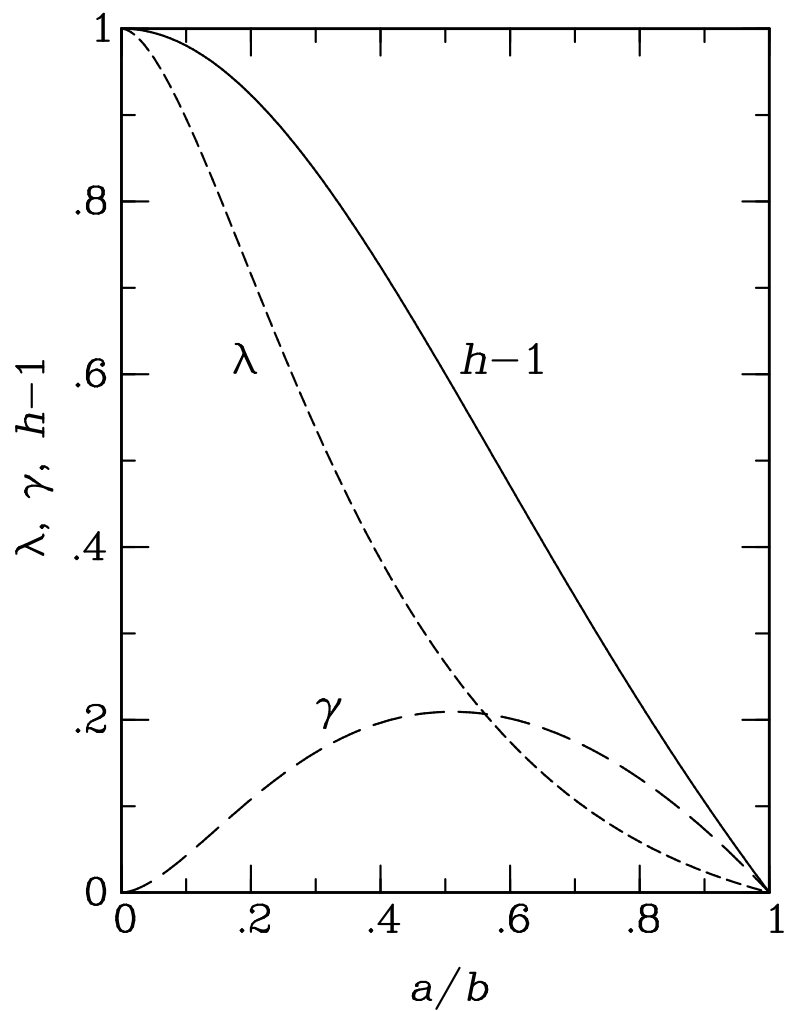


Figure 5

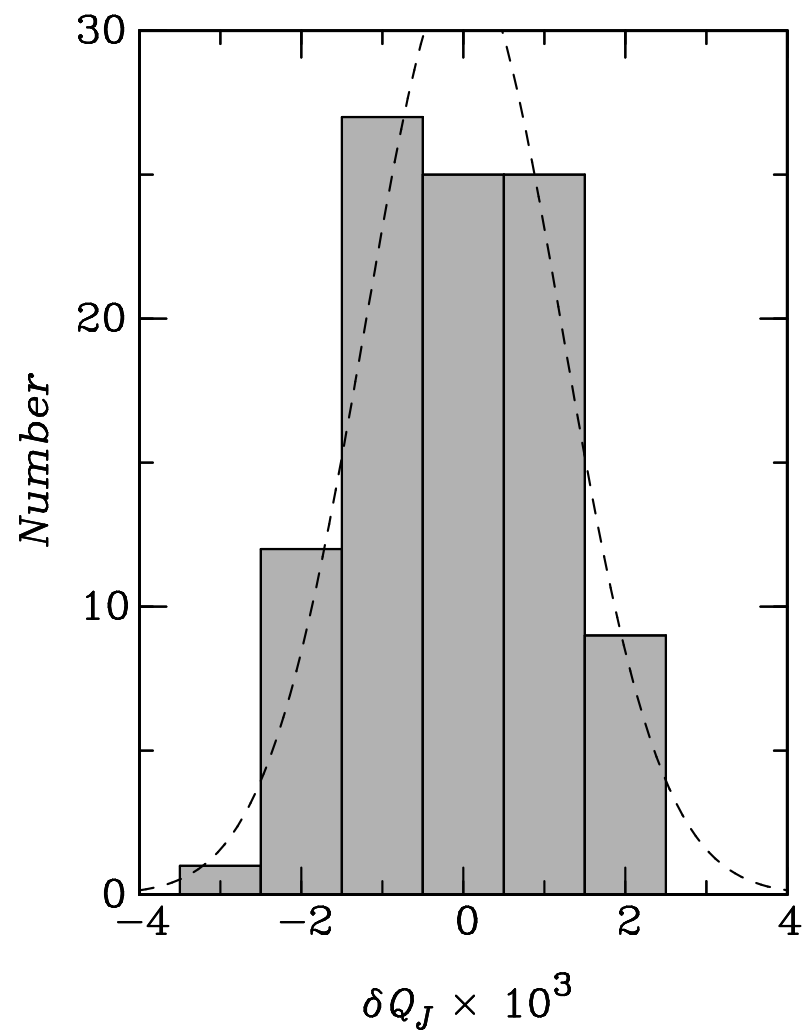


Figure 6

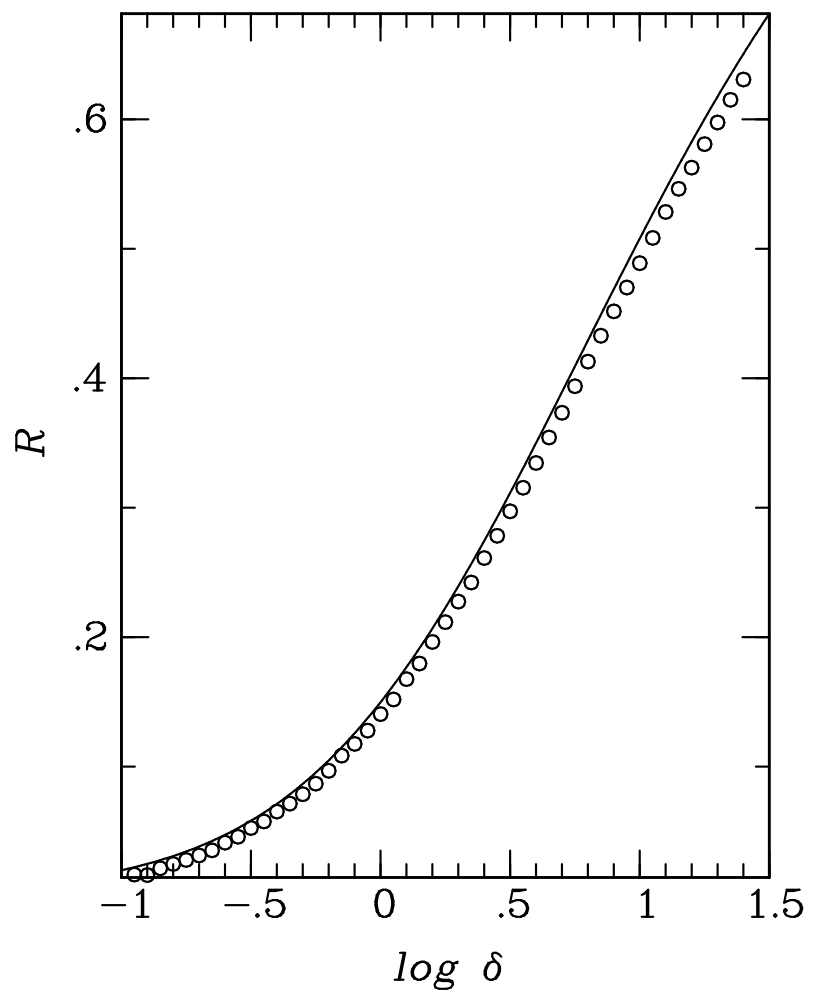


Figure 7

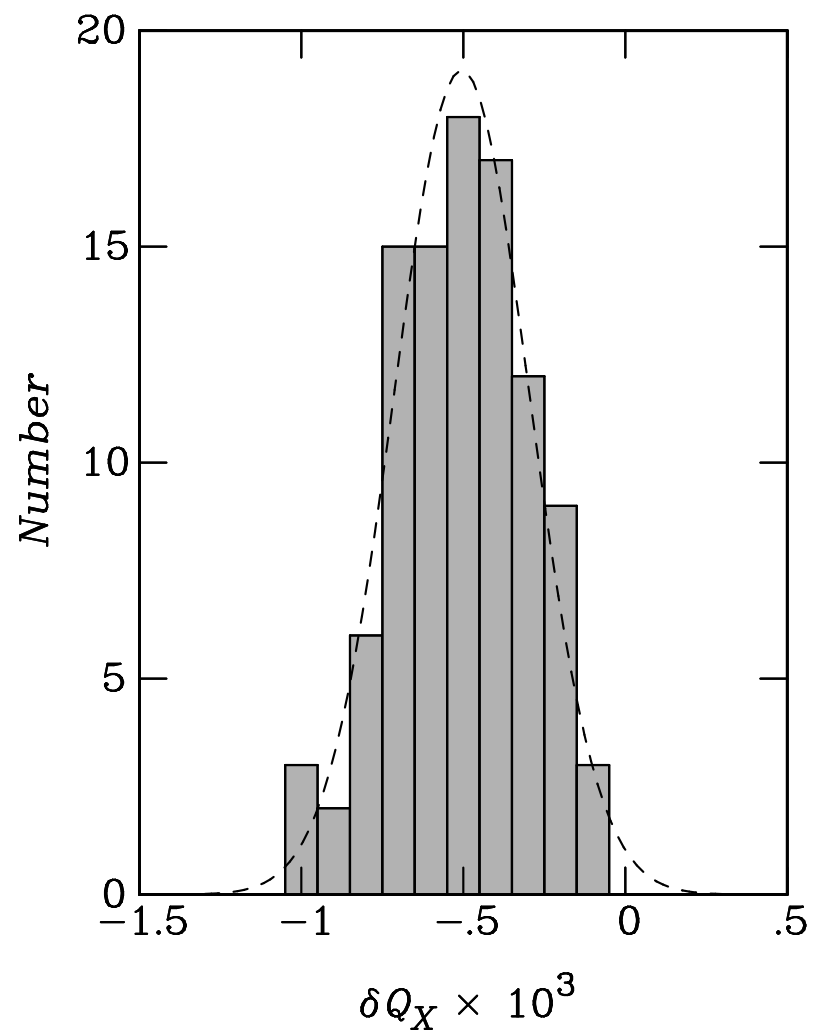


Figure 8

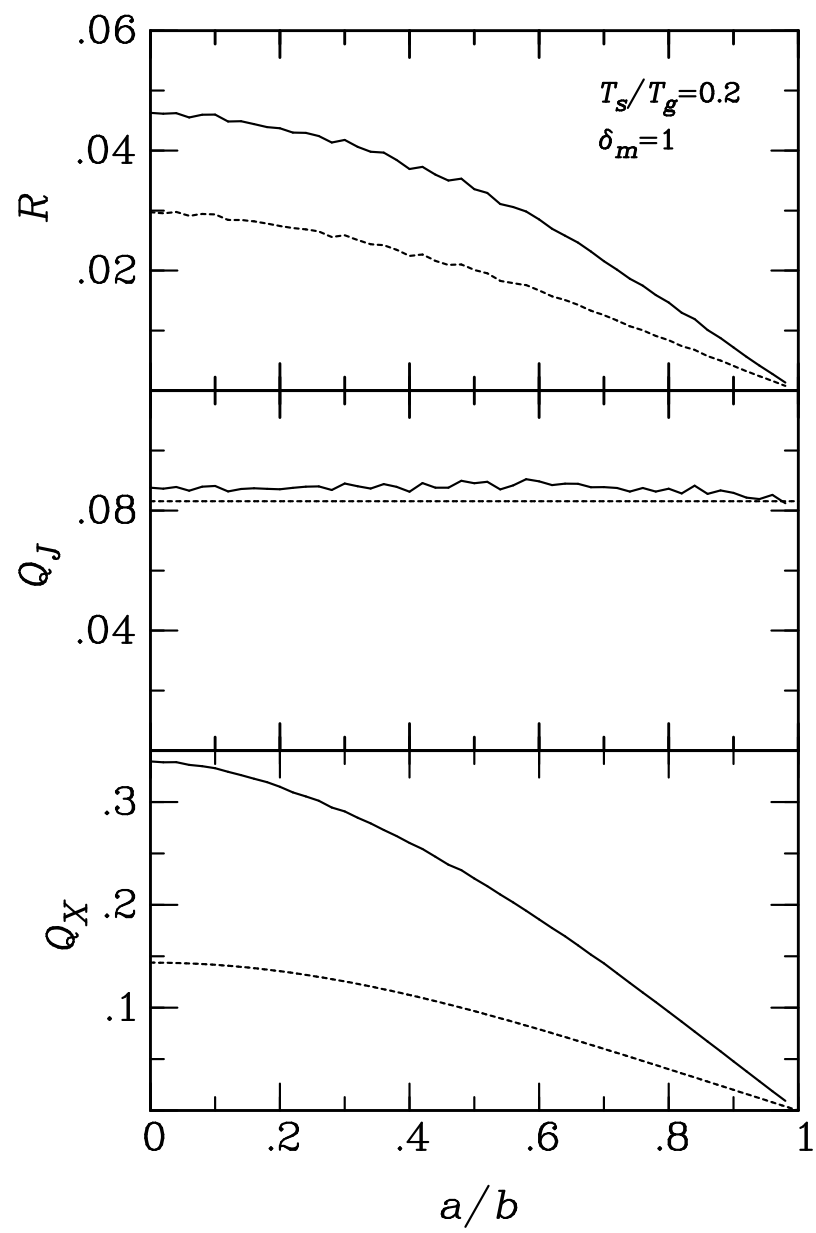


Figure 9a

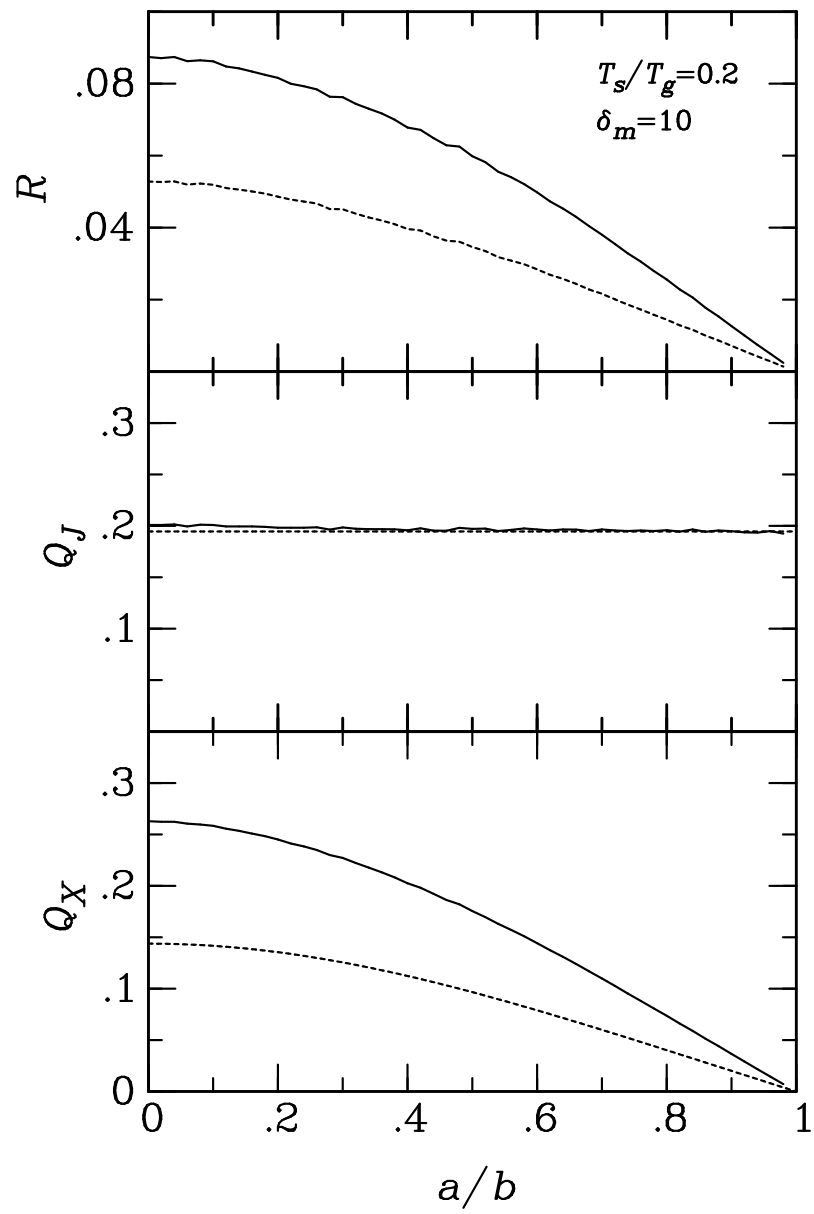


Figure 9b

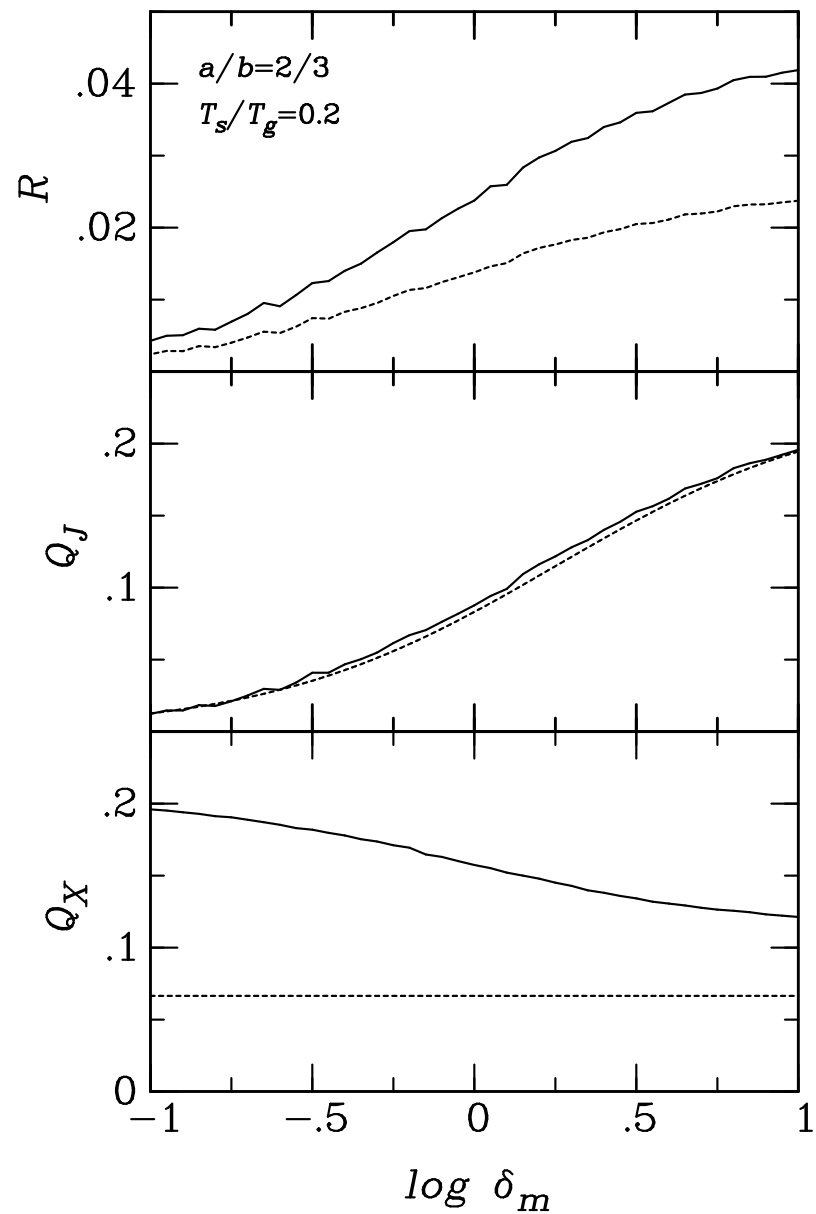


Figure 10

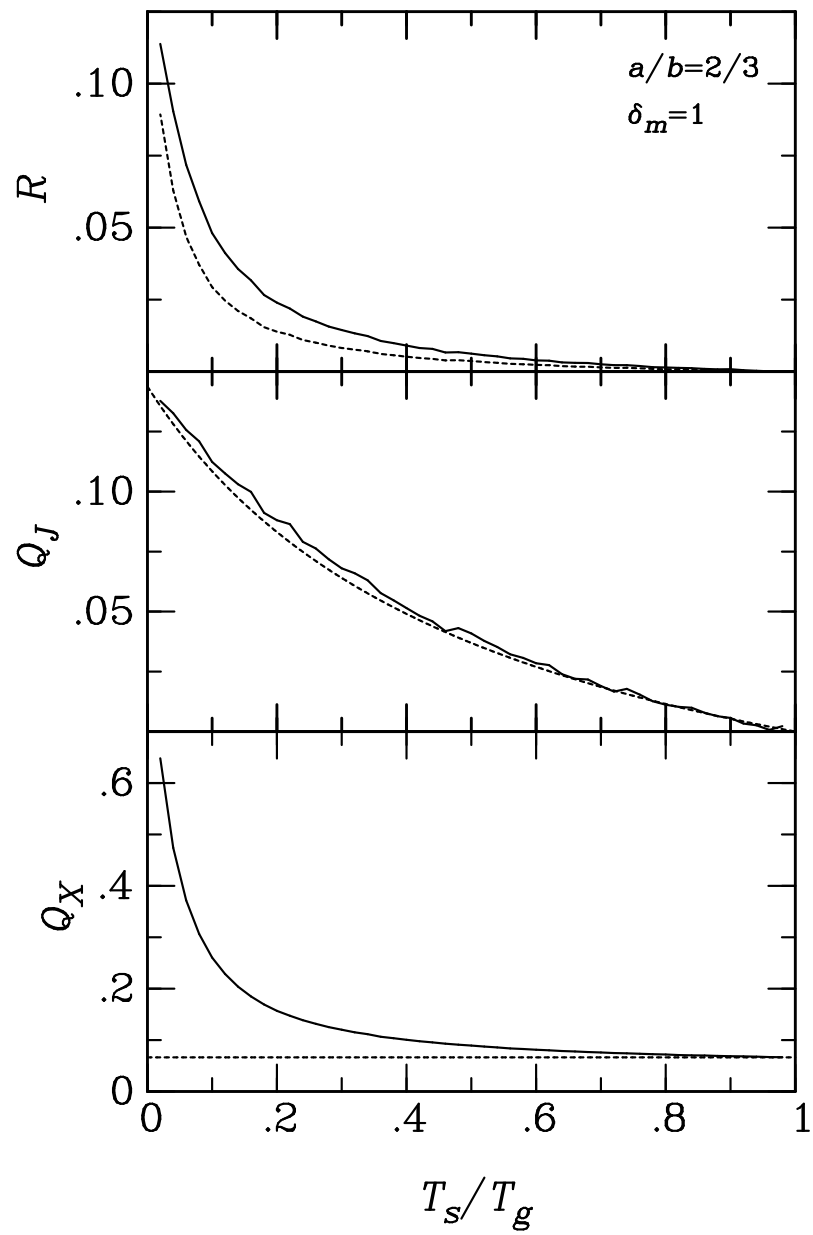


Figure 11a

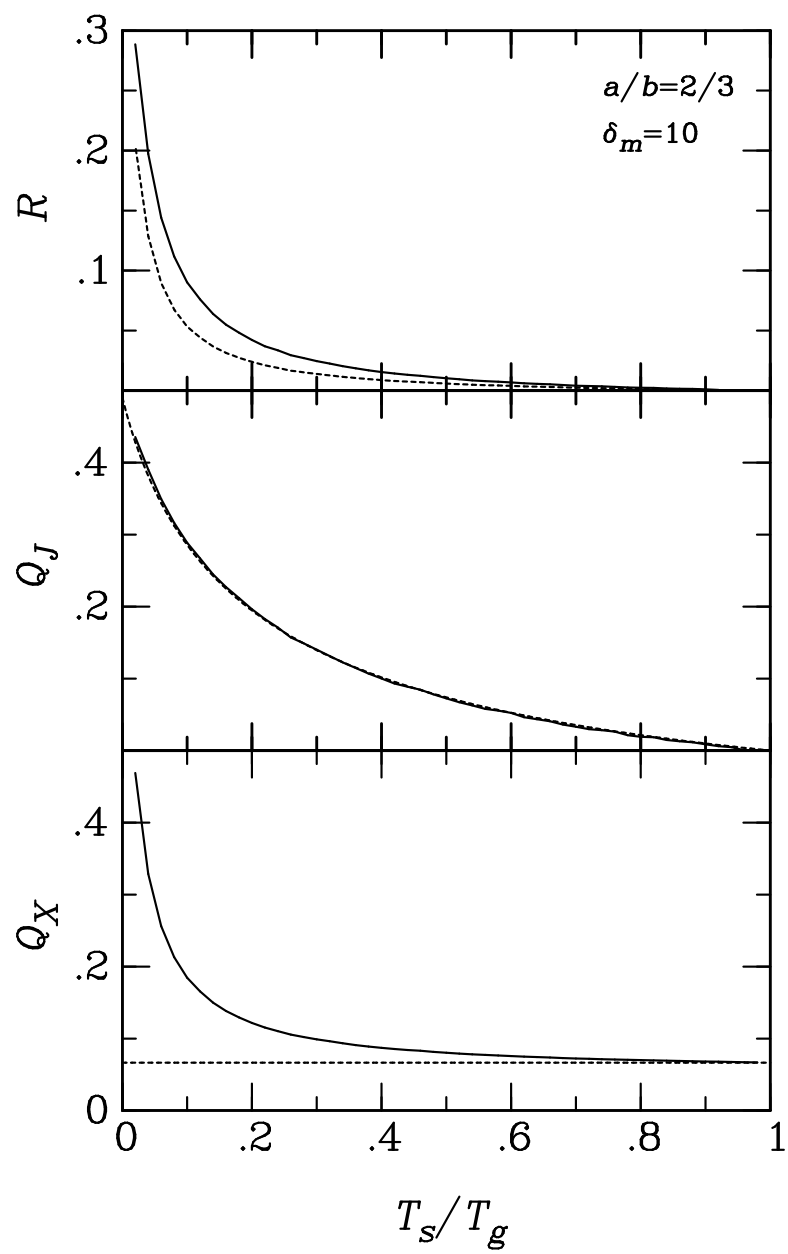


Figure 11b

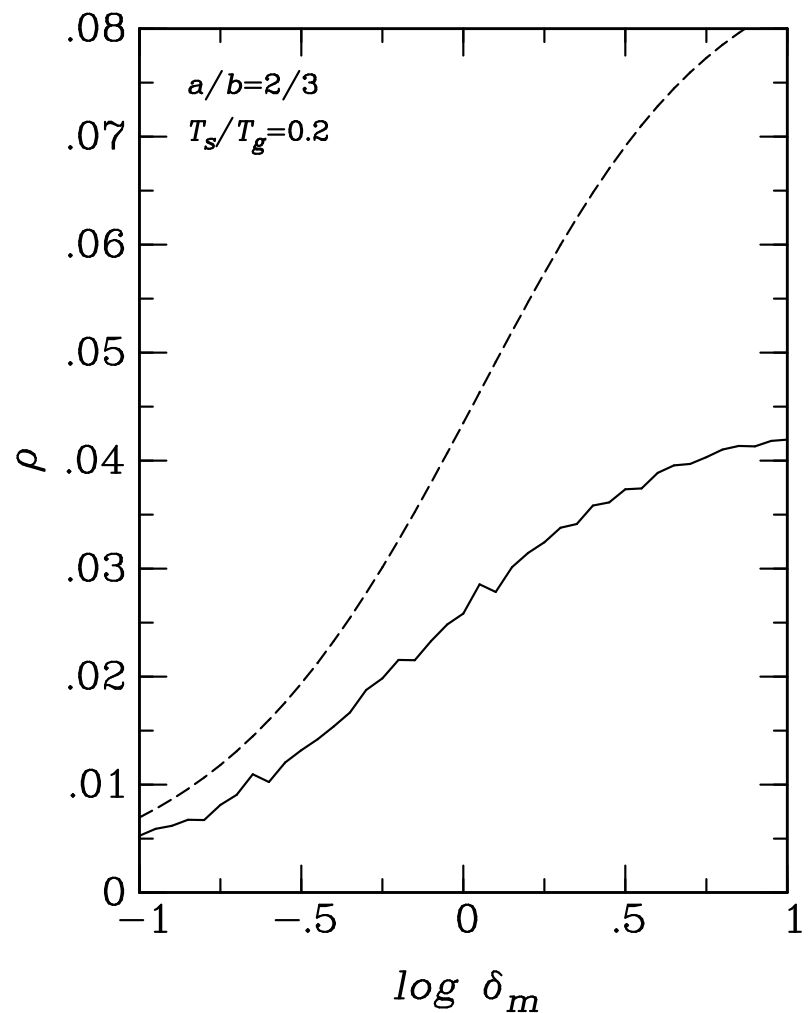


Figure 12

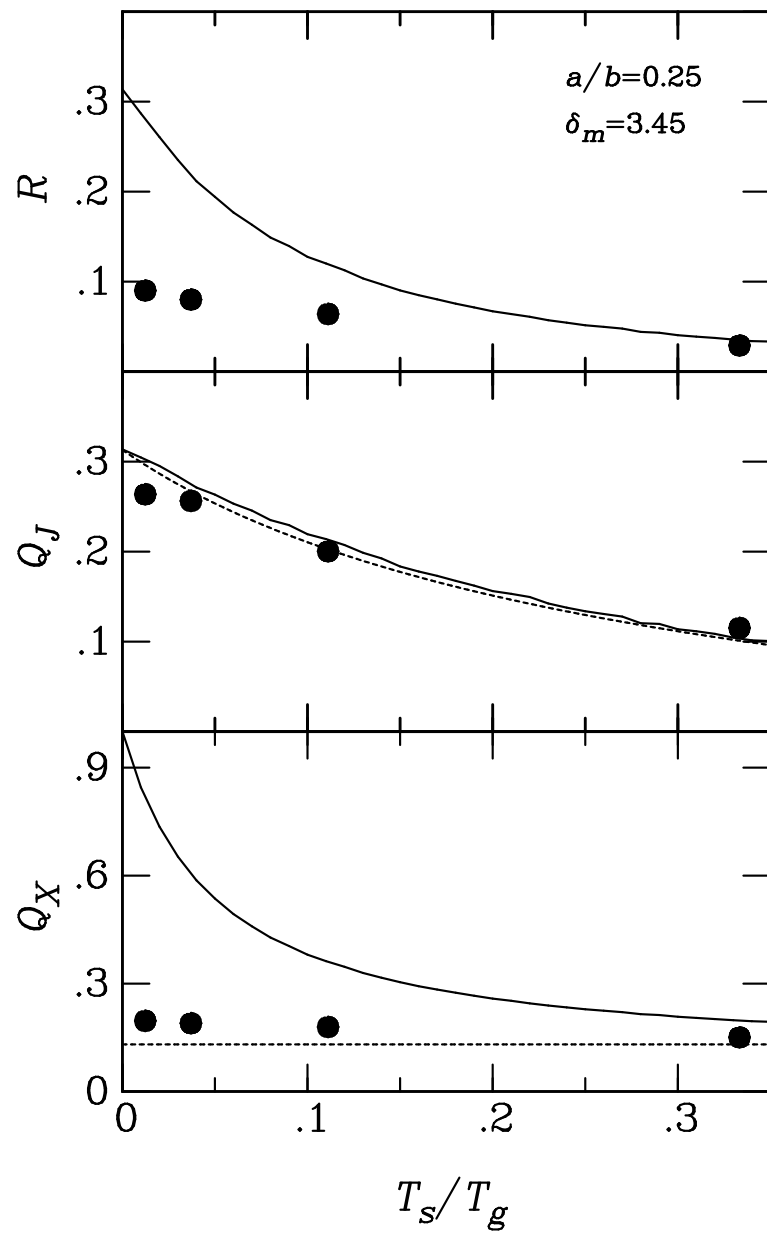


Figure 13

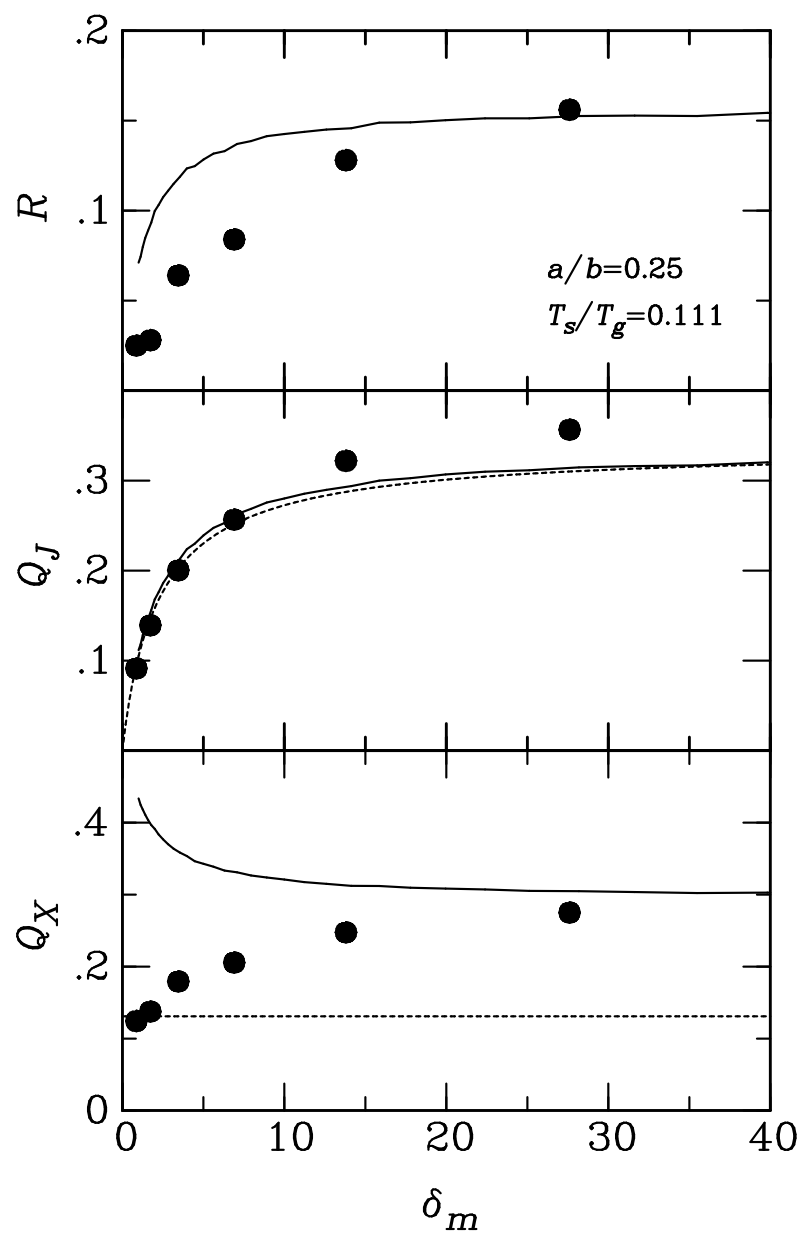


Figure 14